AD-A093 453 BATTELLE COLUMBUS LABS OH F/G 11/6

INVESTIGATING THE EFFECTS OF LOW TEMPERATURE ANNEALING OF AMORP--ETC(U)

NOV 80 R B DIEGLE, D M LINEMAN N00014-77-C-0488

UNCLASSIFIED NL

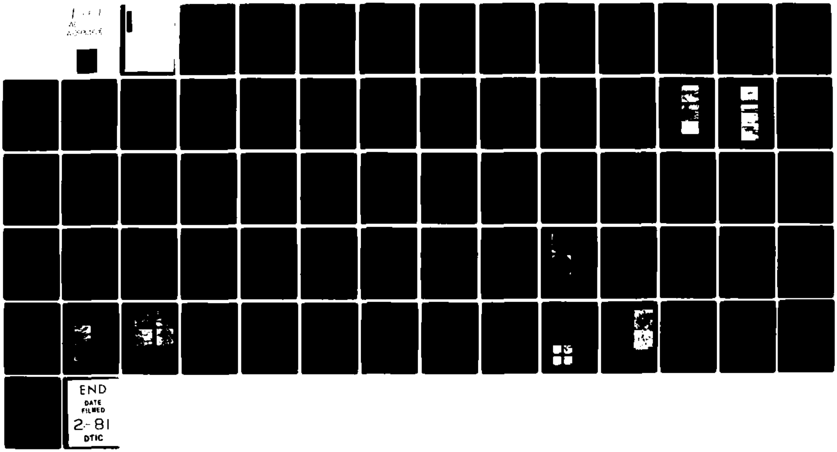

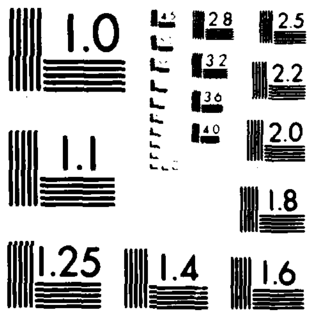

MICROCOPY RESOLUTION TEST CHART

NATIONAL BUREAU OF STANDARDS-1963-A

(12)

OFFICE OF NAVAL RESEARCH

Contract N00014-77-C-0488

FINAL REPORT

For the Period May 1, 1977 to
October 31, 1980

INVESTIGATING THE EFFECTS OF LOW TEMPERATURE ANNEALING OF AMORPHOUS CORROSION RESISTANT ALLOYS

By
R. B. Diegle and D. M. Lineman

Battelle
Columbus Laboratories
505 King Avenue
Columbus, Ohio 43201

9/ Report (Final) 1 May 77 - 31 Oct 80

REPORT DOCUMENTATION PAGE

READ INSTRUCTIONS BEFORE COMPLETING FORM

1. REPORT NUMBER: ONR-00014-77-C-0488-3	2. GOVT ACCESSION NO.: AD-A093 453
3. RECIPIENT'S CATALOG NUMBER	
4. TITLE (and Subtitle): Investigating the Effects of Low Temperature Annealing of Amorphous Corrosion Resistant Alloys	5. TYPE OF REPORT & PERIOD COVERED: Final Report May 1977 – October 1980
	6. PERFORMING ORG. REPORT NUMBER
7. AUTHOR(s): R. B. Diegle ~~and~~ D. M. Lineman	8. CONTRACT OR GRANT NUMBER(s): N-00014-77-C-0488
9. PERFORMING ORGANIZATION NAME AND ADDRESS: Battelle's Columbus Laboratories, 505 King Avenue, Columbus, Ohio 43201	10. PROGRAM ELEMENT, PROJECT, TASK AREA & WORK UNIT NUMBERS: 12 69
11. CONTROLLING OFFICE NAME AND ADDRESS: Procuring Contracting Officer, Office of Naval Research, Dept. of the Navy, 800 N. Quincy St., Arlington, Virginia 22217	12. REPORT DATE: Nov[redacted]980
	13. NUMBER OF PAGES
14. MONITORING AGENCY NAME & ADDRESS (if different from Controlling Office): Defense Contract Administration Services, c/o Defense Electronics Supply Center, Building 5, Dayton, Ohio 45444	15. SECURITY CLASS. (of this report): Unclassified
	15a. DECLASSIFICATION/DOWNGRADING SCHEDULE

16. DISTRIBUTION STATEMENT (of this Report)

Reproduction of this report in whole or in part is permitted for any purpose of the United States Government

DISTRIBUTION STATEMENT A
Approved for public release;
Distribution Unlimited

17. DISTRIBUTION STATEMENT (of the abstract entered in Block 20, if different from Report)

18. SUPPLEMENTARY NOTES

19. KEY WORDS (Continue on reverse side if necessary and identify by block number)

amorphous	segregation	crevice corrosion
annealing	corrosion	pitting
embrittlement	passivity	sputtering

20. ABSTRACT (Continue on reverse side if necessary and identify by block number)

This research program was conducted in two phases. Annealing-induced changes in corrosion and mechanical properties of amorphous alloys were investigated during 1979–80, whereas earlier studies during 1977-1979 involved characterizing the localized corrosion resistance and feasibility of sputtering such alloys.

Annealing, performed at temperatures up to that causing crystallization, produced embrittlement of $Fe_{32}Ni_{36}Cr_{14}P_{12}B_6$ at 100–200 C, as measured by bending. Embrittlement preceded

(Continued)

20. (Continued)

crystallization, which initiated during a substantially higher temperature of 400 C. Annealing of $Fe_{32}Ni_{36}Cr_{14}Si_{6}B_{12}$ resulted in embrittlement at 300–400 C, which coincided with crystallization in this alloy. Segregation of phosphorus is believed to have caused embrittlement of the former alloy, whereas embrittlement of the latter was probably induced by crystallization. Susceptibility of both alloys to corrosion in chloride solutions increased dramatically with the occurrence of crystallization. This increase appeared as a reduction in the critical pitting potential with increasing degree of crystallization.

Research performed during 1977–1979 showed that Fe-Ni-Cr-P-B alloys resist crevice corrosion as well as pitting. This observation was interpreted as indicating that even if initiation of localized corrosion is facilitated by introducing a crevice geometry, corrosion cannot proceed because of the considerable resistance of these alloys to propagation of attack. It was also demonstrated that these alloys can be sputtered as amorphous layers that exhibit essentially the same resistance to pitting corrosion as alloys of similar composition, but prepared by liquid quenching.

ACKNOWLEDGMENTS

The work performed under this contract was supported and monitored by the Office of Naval Research, Metallurgy Program. This support is appreciated, together with that of Dr. Frank Gardner (ONR, Boston), who provided a personal interest in this program.

In addition, the authors are grateful for the assistance of Dr. Dan Merz, of Battelle's Pacific Northwest Laboratories, in preparing the sputtered samples. The authors are also pleased to acknowledge the contributions of R. E. Maringer and R. L. White, Battelle's Columbus Laboratories, for melt spinning amorphous samples and for skillful assistance in scanning electron microscopy, respectively.

ABSTRACT

This research program was conducted in two phases. Annealing-induced changes in corrosion and mechanical properties of amorphous alloys were investigated during 1979-1980, whereas earlier studies during 1977-1979 involved characterizing the localized corrosion resistance and feasibility of sputtering such alloys.

Annealing, performed at temperatures up to that causing crystallization, produced embrittlement of $Fe_{32}Ni_{36}Cr_{14}P_{12}B_6$ at 100–200 C, as measured by bending. Embrittlement preceded crystallization, which initiated during a substantially higher temperature of 400 C. Annealing of $Fe_{32}Ni_{36}Cr_{14}Si_6B_{12}$ resulted in embrittlement at 300–400 C, which coincided with crystallization in this alloy. Segregation of phosphorus is believed to have caused embrittlement of the former alloy, whereas embrittlement of the latter was probably induced by crystallization. Susceptibility of both alloys to corrosion in chloride solutions increased dramatically with the occurrence of crystallization. This increase appeared as a reduction in the critical pitting potential with increasing degree of crystallization.

Research performed during 1977–1979 showed that Fe-Ni-Cr-P-B alloys resist crevice corrosion as well as pitting. This observation was interpreted as indicating that even if initiation of localized corrosion is facilitated by introducing a crevice geometry, corrosion cannot proceed because of the considerable resistance of these alloys to propagation of attack. It was also demonstrated that these alloys can be sputtered as amorphous layers that exhibit essentially the same resistance to pitting corrosion as alloys of similar composition, but prepared by liquid quenching.

TABLE OF CONTENTS

LIST OF TABLES

LIST OF FIGURES

LIST OF FIGURES
(Continued)

BACKGROUND

The advent of amorphous[a] alloys containing film-forming elements such as chromium has led to intensive research into corrosion behavior. One reason for interest in corrosion behavior is the broad similarities of composition between certain amorphous alloys and that of conventional stainless alloys. Specifically, the presence of Fe, Ni, and Cr provides, for the first time, an opportunity for fundamental studies of passivity and its breakdown on stainless-type alloys that are free of conventional long-range crystalline defects, such as grain boundaries.

Previous research showed that two classes of amorphous alloys, of general compositions Fe-Ni-Cr-P-B and Fe-Ni-Cr-P-C, possess remarkable resistance to localized corrosion, namely, pitting.[1-4] Potentiodynamic polarization in acidified chloride electrolytes showed that the critical pitting potential, E_{cp}, was several tenths of a volt more positive than that of conventional crystalline stainless steels of similar chromium content. One group of researchers demonstrated that the minimum amount of chromium needed to confer passivity in the amorphous state was only 8 atomic percent[1], in contrast to the 12 atomic percent required in crystalline stainless steels. These preliminary studies indicated that these new classes of materials constitute novel alloy systems with not only improved corrosion resistance relative to crystalline stainless steels, but also with the promise of conserving chromium, a critical resource.

The favored hypothesis to account for the pitting resistance of amorphous chromium-containing alloys is based on their extremely homogeneous structure. Because the alloys are amorphous, they are free of grain boundaries, stacking faults, dislocations, and other defects found in crystalline structures. Because they are quenched at rates in excess of 10^5 K/sec, they also exhibit less macrosegregation and microsegregation, and they are free of second phases formed by solid state precipitation. At worst, they are somewhat heterogeneous on an atomic scale because of some short range ordering and clustering phenomena. The alloys, therefore, are presumed to resist pitting in part because of the difficulty of initiation. That is, it is well known that pitting occurs preferentially at heterogeneous surface sites such as grain boundaries and second phase particles; the fact that these sites are absent in amorphous alloys is used to rationalize the fact that E_{cp} is several tenths of a volt more noble than in less-perfect alloys. This hypothesis is supported by evidence that passive films formed on Fe-Ni-Cr-P-C alloys are similar in structure to those observed on crystalline stainless steels.[5]

It has also been shown that phosphorus enhances corrosion resistance, presumably by enriching the passive film in hydrated chromium oxyhydroxide.[6] Studies by X-ray photoelectron spectroscopy (XPS) indicate that phosphorus accelerates active dissolution prior to passivation; this acceleration, in turn, promotes enrichment of trivalent chromium in the passive film and improvement of its protective qualities.

(a) "Glassy" would be a more accurate term, since short range order does exist in these materials; however, for the sake of consistency with much of the corrosion literature, the term "amorphous" will be used to denote their noncrystalline structure.

1977–1979 Research

This three-year research program was divided into two phases. The first phase occupied the period from May, 1977 through April, 1979. It was entitled "Investigating Localized Corrosion and Sputtering Feasibility of Amorphous Chromium-Containing Alloys", and research results are documented in References 7-11 and Appendices A, B, and C. One aspect of the research sought to determine whether the resistance to localized corrosion exhibited by certain amorphous alloys extends to crevice corrosion. Crevice corrosion does not require heterogeneities in the alloy for initiation, and oxygen depletion can easily occur within crevices. Therefore, it was wondered whether the alloys might readily corrode in a crevice geometry, unlike their performance when evaluated in a freely exposed geometry. Susceptibility to crevice corrosion was investigated by using actual crevices formed by cold rolling melt spun filaments[12], and also prepared crevices that were instrumented with micro pH and microreference electrodes. This research provided insight into the susceptibility of amorphous Fe-Ni-Cr-P-B alloys to propagation, as well as initiation of localized corrosion.

A second aspect of the 1977–1979 research focused on developing sputtering as a technique for applying amorphous Fe-Ni-Cr-P-B alloys as corrosion resistant coatings. Research was conducted in collaboration with Battelle's Northwest Laboratories, which performed the sputtering, whereas alloy characterization was performed primarily at Battelle's Columbus Laboratories. High and low chromium alloys were sputtered onto substrates at ambient and liquid nitrogen-cooled temperatures, after which their structure and corrosion properties were investigated by a variety of experimental techniques. This work resulted in the development of a procedure for sputtering amorphous alloys that exhibited much of the resistance to localized corrosion that characterizes their liquid quenched counterparts.[11]

1979–1980 Research

The third year of research under the present contract was directed toward changes that occur in amorphous chromium-containing alloys during annealing at temperatures up to the crystallization temperature. It sought to determine the changes in properties, both mechanical and chemical, that occur as a result of thermally induced structural relaxation. In particular, it addressed the question of whether the response of chemical stability to annealing parallels that of mechanical properties, indicating a possible common cause for the changes, or whether the responses differ and occur as the result of different types of annealing-induced relaxations.

Naka, et al.[13] investigated the isothermal annealing response of amorphous $Fe_{70}Cr_{10}P_{13}C_7$ and $Fe_{32}Ni_{36}Cr_{14}P_{12}B_6$ alloys and found that they crystallized in two stages. The first phase to appear was designated MSI, which is a metastable FCC solid solution of Ni, Fe, and Cr with Ni as the major constituent. The next phase to appear also was metastable, designated MSII, and it was possibly a mixture of metal-metalloid compounds with order structures. MSI formed as crystallites of 50 nm maximum diameter, and MSII nucleated around these MSI crystallites. After disappearance of the amorphous phase due to the formation of MSI and MSII, further transformation resulted in stable phases by diffusion and recrystallization, and/or decomposition of metastable phases. Anodic polarization studies showed that formation of MSI lowered the corrosion potential and increased the current density in the passive potential range for the $Fe_{32}Ni_{36}Cr_{14}P_{12}B_6$ alloy. The current density in the active and passive potential ranges increased continuously as MSI and MSII phases underwent growth by heat treatment for

increasing time intervals. Appearance of MSII accelerated transpassive corrosion, probably because it was enriched in chromium. Results of other studies[14,15] of $Fe_{32}Ni_{36}Cr_{14}P_{12}B_6$ amorphous alloy also showed a two-stage crystallization process. Crystallization was detected by differential thermal analysis and microhardness measurements at ~350 C with isothermal annealing. The first phase, MSI, was an FCC, Ni-rich Ni and Fe solid solution that grew by diffusion control. MSII began to appear at an annealing temperature of about 390 C, and it grew at a linear rate with time. It probably nucleated at the phase boundaries between existing MSI crystals and the amorphous matrix. It possessed a metalloid/metal ratio of 1:3 and thus was enriched in metalloid components. However, research with $Fe_{40}Ni_{40}P_{14}B_6$ indicated that low temperature (350–370 C) annealing produced an Fe_3P type bct structure with a small amount of FCC Ni-Fe solid solution and a small amount of α-Fe. Walter and Bartram[16] later concluded that the metalloid plays an all-important role in determinng the nature of crystals formed in amorphous alloys containing various amounts of P and B.

Research with Cu-Zr amorphous alloys[17] addressed the influence of crystal structure on corrosion reactions. Annealing below T_c was not performed; rather, the comparison was between the as-quenched amorphous and the fully crystallized structures. Crystallization to a nearly single phase produced a positive shift in corrosion potential, suggesting that reduced cathodic kinetics account for the higher corrosion resistance of the amorphous state. Crystallization to a two-phase alloy also resulted in a less electronegative corrosion potential than that of the amorphous alloy. The crystalline alloys corroded more rapidly than their amorphous counterparts, and the two-phase crystalline material corroded less rapidly than the single-phase crystalline alloy. The reduced corrosion rate may have occurred because of the greater Zr content in the former material, since Zr has a lower exchange current density for the hydrogen reaction.

Embrittlement of amorphous alloy $Fe_{40}Ni_{40}P_{14}B_6$ was found to occur when heated above 100 C for two hours.[18] Annealing at 325 C and 350 C resulted in phosphorus on the fracture surfaces at levels of twice that of the bulk composition. Ion milling to a depth of about 6 nm reduced the phosphorus concentration to near that of the bulk alloy. It was concluded that the phosphorus-enriched regions caused the embrittlement, and possibly served as nuclei for subsequent crystallization. Auger analysis of the melt spun filaments showed phosphorus enrichment near the shiny ribbon surface. Related studies[19] with amorphous alloys $Fe_{40}Ni_{40}B_{20}$, $Fe_{50}Ni_{30}P_{14}B_6$, and $Fe_{50}Ni_{30}B_{20}$ involved ductility measurement by a simple bend test. Removal of phosphorus as a metalloid component suppressed embrittlement, i.e., higher annealing temperatures were required to embrittle phosphorus-free alloys. It was concluded that "replacement of P by B inhibits the low-activation processes involved in the embrittlement process". The temperature for the onset of embrittlement differed by nearly 150 C due to the influence of phosphorus.

Microhardness experiments performed with Fe-Ni-base amorphous alloys showed two maxima for annealing temperatures below about 450 C.[20] For the $Fe_xNi_{80-x}P_{14}B_6$ alloys in the as-quenched condition, microhardness values were approximately 900 Kp mm^{-2}. Hardness maxima were observed both above and below T_c, the crystallization temperature, which was about 400 C, and the maxima were higher above T_c. The appearance of metastable phases and their disappearance on annealing caused the higher maxima; these phases were of the A_3B type and were isomorphous with Fe_3P crystal structures. The appearance of hardness maxima below T_c was interpreted as indicating structural changes in the amorphous state, and therefore preceding those occurring as a result of crystallization.

The effect of annealing and hydrogen charging on fractography of Fe-Cr-Mo-C alloys was investigated by Kawashima, et al.[21] They found that the crack velocities and fracture surfaces of alloys embrittled by heat treatment were similar to those of alloys embrittled by hydrogen. Wallner lines, characteristic of fracture surfaces of completely brittle solids, were observed as a result of both annealing and hydrogen charging. However, a crystallized specimen showed a granular type of fracture surface, suggesting intergranular failure. It was concluded that the mechanisms of crack propagation are essentially the same in materials embrittled by annealing and by hydrogen charging.

The research described in this report had two purposes. One was to characterize the differences in annealing response of changes in corrosion properties relative to changes in other properties, primarily mechanical. The second was to determine the role of phosphorus in influencing both types of responses. Results of the 1979–1980 research are presented in detail in this report, whereas results from 1977–1979 work are described in Appendices A–C. The implications of all three years of research to understanding corrosion of amorphous alloys are presented in the Discussion section.

MATERIALS AND PROCEDURES

Materials

The alloy compositions used in this research are listed in Table 1. The major compositional variables were Cr and P. The 14Cr alloy obtained from Allied Chemical Corporation is similar in composition to the 16Cr Battelle alloy, but represents material produced at another laboratory. The composition containing 12 atomic percent B and 6 atomic percent Si was evaluated as representative of a non-phosphorus containing alloy. The V was present as an unintentional impurity that was introduced through use of a ferrophosphorus compound. T304 stainless steel was included as an example of a commercial stainless steel. Incoloy 800 was evaluated because the Fe, Ni, and Cr levels approximated those in the 16 atomic percent Battelle alloy, but they were present in a crystalline rather than an amorphous structure. Thus, the combined effect of these three elements in the approximate concentrations and ratios present in Incoloy 800 could be studied in both crystalline and amorphous alloys.

The Battelle alloys were first cast into pancake-shaped ingots by conventional casting techniques involving induction melting of pure components in a controlled atmosphere. Next, 30-gram portions from each of the crystalline ingots were removed and melt spun into amorphous filaments.[7] Compositions were verified by wet chemical analysis. Structures were characterized by differential scanning calorimetry (DSC), X-ray diffraction (XRD), and in some cases, by transmission electron microscopy (TEM) of thin foils.

TABLE 1. COMPOSITIONS OF ALLOYS USED IN RESEARCH PROGRAM

Preparation Technique	Source	Amorphous	Composition, atomic percent Fe	Ni	Cr	V	P	B	Si	C	Mn	Ti
Melt spinning	Battelle	Yes	45	30	2	2	15	6				
		Yes	42	30	5	2	15	6				
		Yes	40	30	7	2	15	6				
		Yes	37	30	10	2	15	6				
		Yes	31	30	16	2	15	6				
		Yes	32	36	14			12	6			
Melt spinning	Allied	Yes	40	40	0		14	6				
		Yes	32	36	14		12	6				
Sputtering	Battelle	Yes	45	30	2	2	15	6				
		Yes	31	30	16	2	15	6				
Conventional (casting and rolling)	Mill	No	69	8	20				1.2	0.00	1.7	(T304 stainless steel)
		No	46	31	22					0.00		0.008 (Incoloy 800)

Procedures

Annealing

Filaments were sealed into evacuated quartz ampoules and annealed isothermally in a tube furnace. An ampoule was inserted into the center of the preheated furnace, and the temperature (monitored by a thermocouple placed next to the ampoule) was allowed to return to the set value. When it was within about 5 C of the set value, the time interval for the anneal was begun. At the end of the interval, which in most cases was one hour, the ampoule was removed from the furnace and cooled in air, after which it was broken open and the contents removed.

Ductility was measured by bending the filaments in the shape of a U between parallel glass plates which were mounted on the jaws of a small pin vise. The jaws were slowly closed until the filament fractured, at which point the plate separation was carefully measured with a micrometer. Usually at least three fracture measurements were made for a given specimen condition. Care was taken to ensure that the same ribbon surface, either shiny or dull, was maintained outward during a series of measurements, as this factor was found to influence

results. Ductility was measured as the strain, γ, in the outer fiber surface, which is given by the equation

$$\gamma = \frac{t}{2r-t} \quad , \tag{1}$$

in which 2r is the plate separation distance and t is the filament thickness. The strain at fracture, γ_f, was used as a measure of ductility. It should be mentioned that this equation is strictly valid only before yielding occurs, but it also provides a useful approximation of strain at small plastic strains.

XRD measurements were performed with a Siemens unit at an angular scan rate of one degree per minute. The instrument was first calibrated against a gold standard, and CrKα radiation was used for all measurements.

Vickers hardness measurements were made on the shiny surfaces of filaments that were glued to glass slides. A very thin layer of glue was used, and its presence did not substantially affect the hardness transitions that were being evaluated. Indenter loads from 20 to 100 g were investigated, and a load of 50 g was adopted for all subsequent hardness measurements.

Corrosion behavior was evaluated primarily by potentiodynamic polarization, as described previously.[8] Some experiments involved potentiodynamically polarizing electrodes to predetermined potentials and recording the current-time response. Some gravimetric measurements also were performed, in which the weight losses of preweighed filaments were determined after exposure in $FeCl_3$ solution in open beakers for many hours.

RESULTS

X-Ray Diffraction

Essentially no changes in XRD data were observed for amorphous $Fe_{32}Ni_{36}Cr_{14}P_{12}B_6$ alloy as a result of annealing to 375 C for one hour, as shown in Figure 1. A one-hour anneal at 400 C (data not shown) did result in several X-ray intensity peaks that could be indexed with those of MSI, namely, an FCC solid solution of FeNi. No other phases were detected.

Annealing at 425 C resulted in a series of diffraction peaks corresponding to either of two crystalline phases. MSI, an FeNi solid solution and probably also containing Cr[14,15], with a = 0.36 nm appeared as indicated by the three diffraction peaks. (Additional peaks, not shown in Figure 1, were detected at smaller 2θ values with CuK$_\alpha$ radiation.) Also present were peaks corresponding approximately to the Ni_3P-type compound designated MSII.[14,15] In the Metglas alloy system MSII probably has a general composition of the type $(Ni,Cr,Fe)_3(P,B)$. The final equilibrium stage, SIII, presumably was not present because higher annealing temperatures are required for its formation.[14]

The effects of annealing alloy $Fe_{32}Ni_{36}Cr_{14}Si_6B_{12}$ are shown in Figure 2. Fewer diffraction peaks are present for this non-phosphorus containing alloy, relative to Metglas 2826A depicted in Figure 1. The peaks developed at an anr ·aling temperature between 400 and 500 C and their positions correspond to an FeNi-type of compound with a = 0.36 nm. This phase is probably the

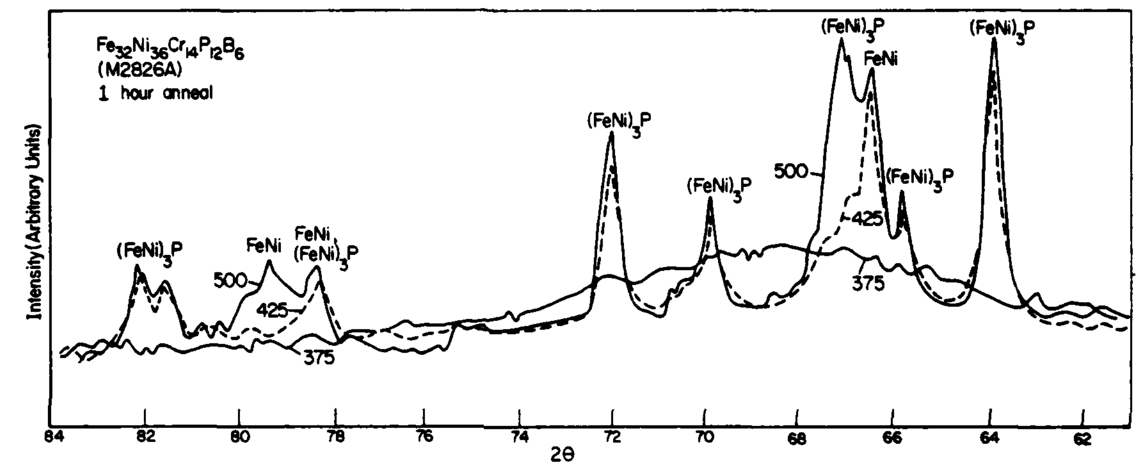

FIGURE 1. X-RAY DIFFRACTION RESULTS FROM $Fe_{32}Ni_{36}Cr_{14}P_{12}B_6$ ANNEALED FOR ONE HOUR AT VARIOUS TEMPERATURES (Cr K_α RADIATION)

Alloy was commercial Metglas 2826A.

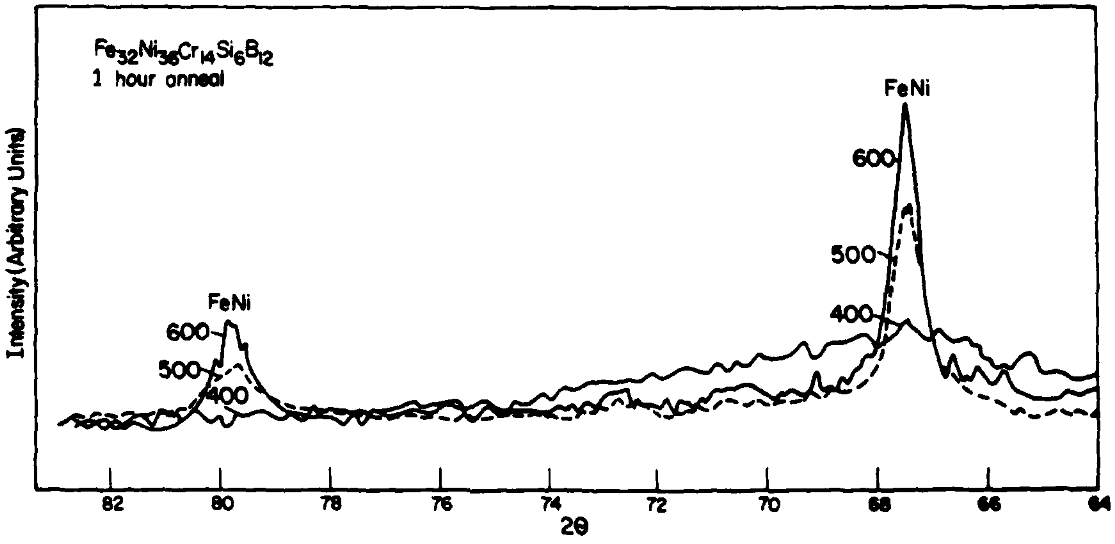

FIGURE 2. X-RAY DIFFRACTION RESULTS FROM $Fe_{32}Ni_{36}Cr_{14}Si_6B_{12}$ ANNEALED FOR ONE HOUR AT VARIOUS TEMPERATURES (Cr K_α RADIATION)

Alloy was prepared at Battelle.

counterpart of MSI found in Metglas 2826A. Peaks suggestive of an MSII phase, in which the metalloid content of the $(Ni,Cr,Fe)_3(P,B)$-type compound consists only of Si and/or B, were not detected.

X-ray diffraction data taken from as-cast ingots of compositions identical to those of the P-and Si-containing described above consisted of numerous peaks that could not be identified with certainty. It appears that an FeNi-type solid solution compound was present in both ingot compositions, but other, less readily identifiable phases were also detected. Complicated structures for SIII are anticipated, based on the previous work by von Heimendahl and Maussner.[14]

Differential Scanning Calorimetry

Differential scanning calorimetry (DSC) data, Table 2, for $Fe_{32}Ni_{36}Cr_{14}P_{12}B_6$ showed two exothermic peaks corresponding to the formation of MSI and MSII phases. The temperatures at which these phases began to form are 404 and 442 C, in reasonable ageement with those measured in another investigation.[14] The heats of reaction, 6.3 and 7.3 cal/g for MSI and MSII, respectively, were of comparable magnitude. An amorphous alloy of composition $Fe_{31}Ni_{30}Cr_{16}P_{15}B_6$ and prepared by sputtering showed only one exothermic peak, unlike the melt spun alloy of similar composition. Alloy $Fe_{32}Ni_{36}Cr_{14}Si_6B_{12}$ produced only one exothermic peak at a temperature of 526 C and with an enthalpy of 8.0 cal/g. This temperature is substantially greater than that for MSI of $Fe_{32}Ni_{36}Cr_{14}P_{12}B_6$, indicating greater thermal stability toward crystallization of the P-free alloy.

TABLE 2. RESULTS OF DIFFERENTIAL SCANNING CALORIMETRY MEASUREMENTS[a]

Alloy Composition	Transition Temperatures, °C	Δ H, cal/g
$Fe_{32}Ni_{36}Cr_{14}P_{12}B_6$	404	6.3
	442	7.3
$Fe_{32}Ni_{36}Cr_{14}Si_6B_{12}$	526	8.0
$Fe_{31}Ni_{30}Cr_{16}V_2P_{15}B_6$ (sputtered)	467	8.7

(a) Temperature scan rate = 5 C/min.

Ductility Measurements

Figure 3 shows the variation of fracture strain, γ_f, of $Fe_{32}Ni_{36}Cr_{14}P_{12}B_6$ with annealing temperature during room temperature bend testing. Fracture occurred at higher strains if the convex surface of the specimen was the shiny (air side) surface; the difference in ductility was small at large fracture strains, but it became substantially greater as the degree of embrittlement increased. Embrittlement became detectable in the temperature range 100–200 C and resulted in a substantial loss in ductility. It progressed more slowly in the temperature range 200–500 C and was nearly complete at 500 C. The transition in embrittlement was relatively uniform and did not indicate the concurrent phenomenon of crystallization of metastable phases. The shiny side of $Fe_{32}Ni_{36}Cr_{14}Si_6B_{12}$ filaments also showed a slower rate of embrittlement, Figure 4. Variability between behavior of the two surfaces was greater in the lower temperature range than that observed with $Fe_{32}Ni_{36}Cr_{14}P_{12}B_6$. Embrittlement (measured with the shiny surface outward) initiated in the temperature range 400–500 C, or 300 C higher than that of the P-containing alloy. It proceeded over a relatively narrow temperature range of about 100 C and was nearly complete at 500 C.

$Fe_{31}Ni_{30}Cr_{16}V_2P_{15}B_6$ was evaluated to determine the degree to which alloy preparation at another laboratory, namely Battelle, under presumably somewhat different quenching conditions influenced embrittlement behavior. The results shown in Figure 5 indicate a higher temperature range for rapid embrittlement relative to that for $Fe_{32}Ni_{36}Cr_{14}P_{12}B_6$ by about 100 C, followed by embrittlement to a minimum γ_f of about 0.008. Because of unintentional differences in composition between the two alloys, closer comparison of embrittlement response is not appropriate.

Figure 6 shows that the ductility of the as-sputtered deposit of $Fe_{31}Ni_{30}Cr_{16}V_2P_{15}B_6$ was 0.038, which was substantially less than the fracture strain of 1.0 for this alloy prepared by melt spinning (Figure 5). Embrittlement of the alloy was virtually complete at an annealing temperature of 300 C, whereas the melt spun filament was not fully embrittled at this temperature. Also, the degree of embrittlement of the deposit was slightly greater, $\gamma_f = 0.004$ as compared to $\gamma_f = 0.006$ for the melt spun alloy.

The transition in fractographic behavior caused by annealing is presented in Figure 7 for $Fe_{32}Ni_{36}Cr_{14}P_{12}B_6$. The fracture surface of the as-cast alloy, Figure 7a, shows evidence of a vein-like pattern caused by shear rupture resulting from plastic instability. The larger features surrounding the central veined region may have resulted from a fatigue effect caused by bending the specimen to induce fracture. Figure 7b shows that annealing at 300 C virtually eliminated the vein pattern, presumably the result of embrittlement. The features in Figure 7c are less pronounced, indicative of a greater contribution of brittle cleavage fracture caused by annealing at a higher temperature of 375 C. Higher temperature anneals resulted in fracture surfaces (not shown) that exhibited very few features except brittle cleavage facets.

The influence of annealing on the fractography of $Fe_{32}Ni_{36}Cr_{14}Si_6B_{12}$ is shown in Figure 8. Features indicative of substantial deformation are evident in Figure 8a for as-cast alloys, although no vein-like structures could be found. Ductile behavior, including features suggestive of a vein-like feature, was evident in Figure 8b, representing a 400 C/2 hour anneal. A granular appearance is evident in Figure 8c, corresponding to a 600 C/1 hour anneal, and is reminiscent of intergranular fracture.

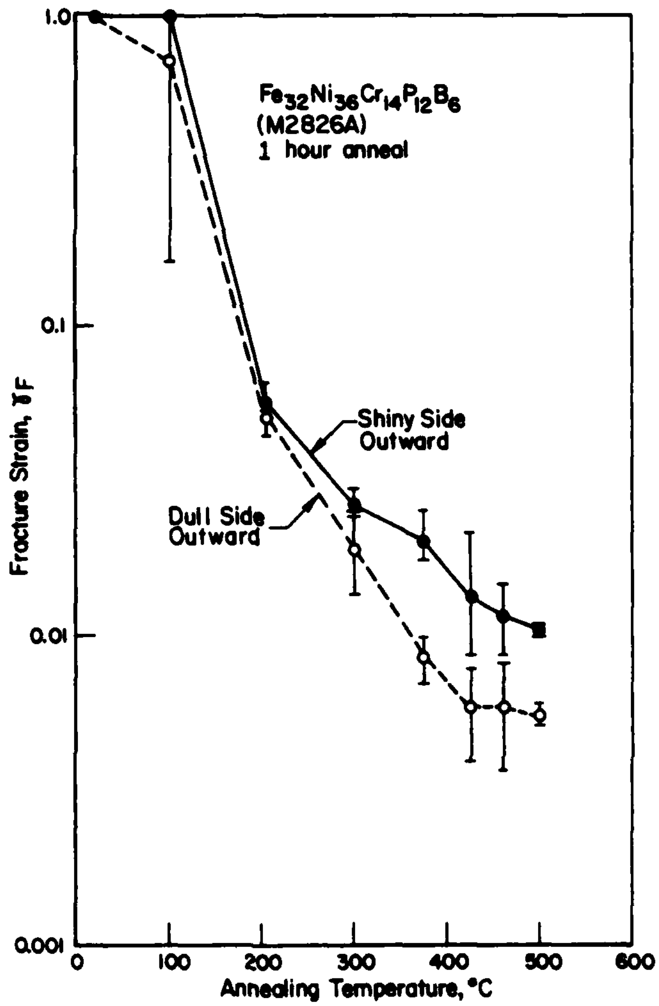

FIGURE 3. FRACTURE STRAIN VERSUS ANNEALING TEMPERATURE FOR $Fe_{32}Ni_{36}Cr_{14}P_{12}B_6$

Measurements were made with both shiny and dull surfaces in tension during bending.

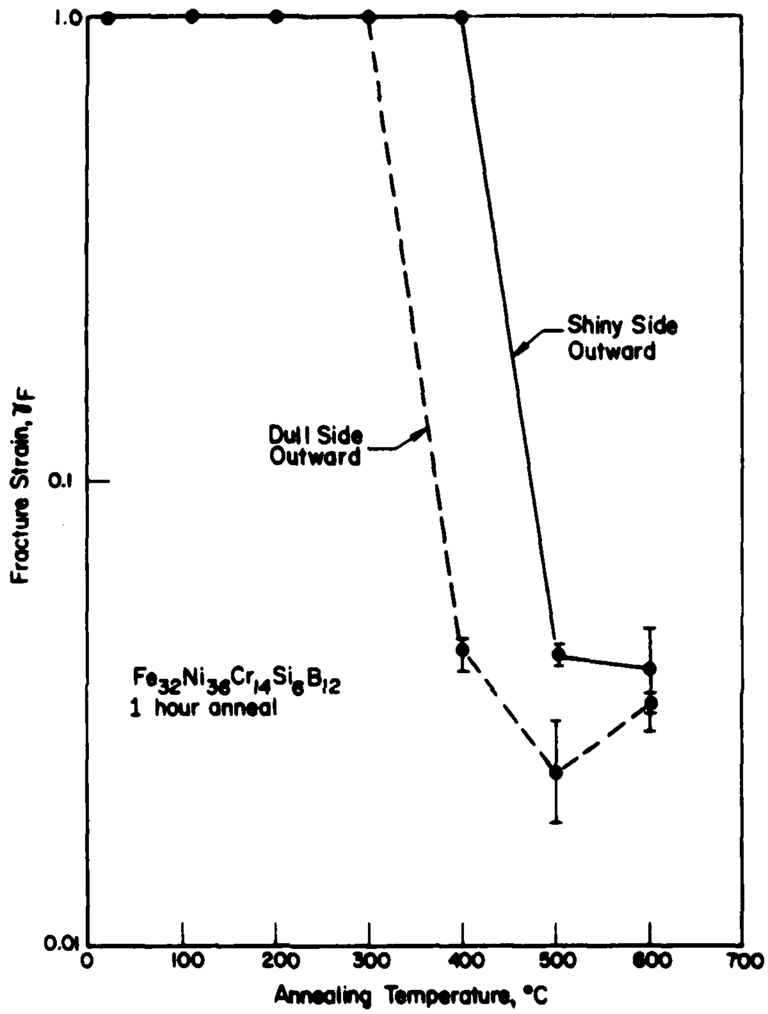

FIGURE 4. FRACTURE STRAIN VERSUS ANNEALING TEMPERATURE FOR $Fe_{32}Ni_{36}Cr_{14}Si_6B_{12}$

Measurements were made with both shiny and dull surfaces in tension during bending.

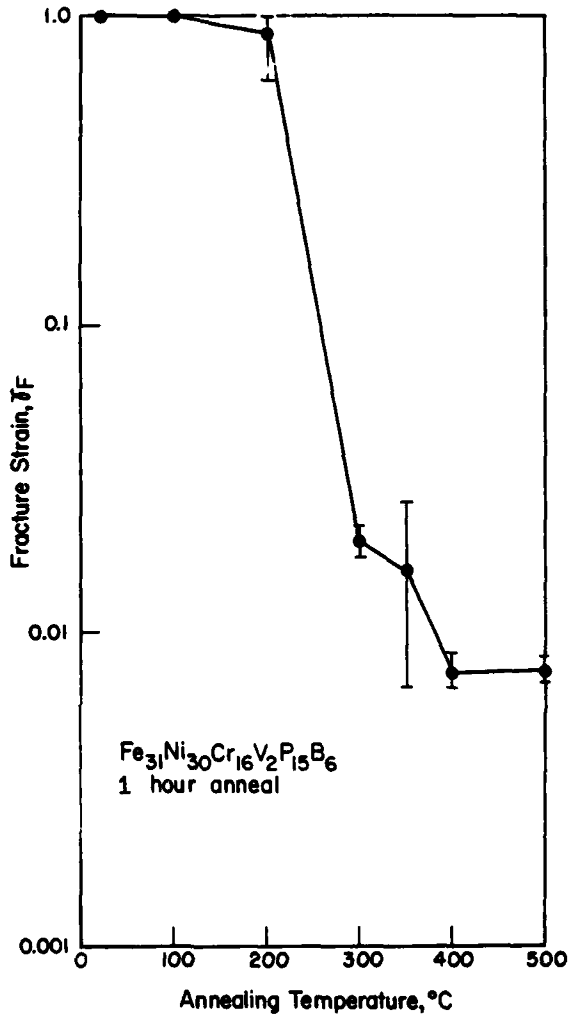

FIGURE 5. FRACTURE STRAIN VERSUS ANNEALING TEMPERATURE FOR $Fe_{31}Ni_{30}Cr_{16}V_2P_{15}B_6$

Measurements were made with shiny surface in tension. Alloy was prepared at Battelle.

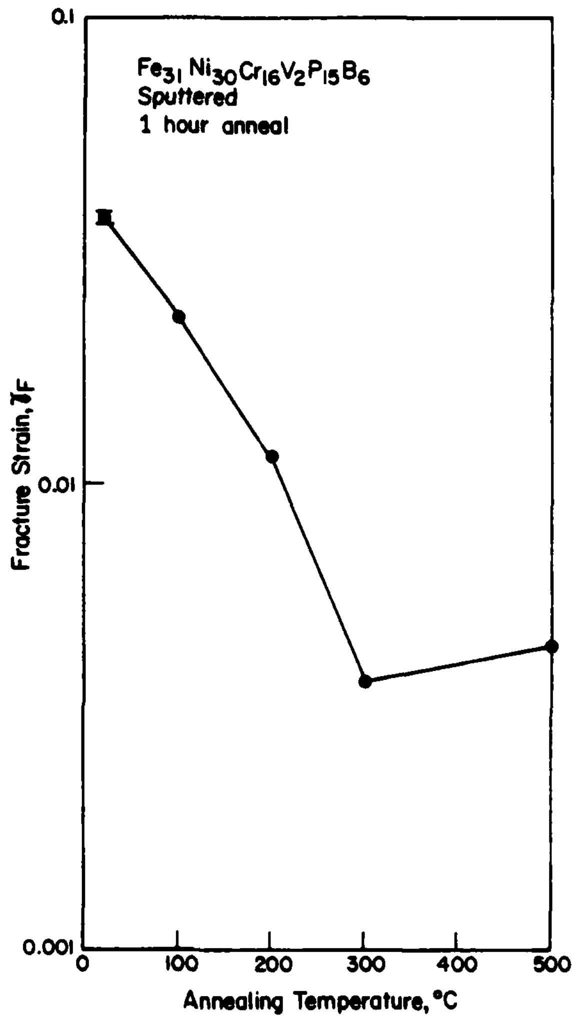

FIGURE 6. FRACTURE STRAIN VERSUS ANNEALING TEMPERATURE FOR $Fe_{31}Ni_{30}Cr_{16}V_2P_{15}B_6$ PREPARED BY SPUTTERING

Measurements were made with the surface that was originally in contact with the substrate in compression. Alloy was sputtered at Battelle Northwest Laboratories.

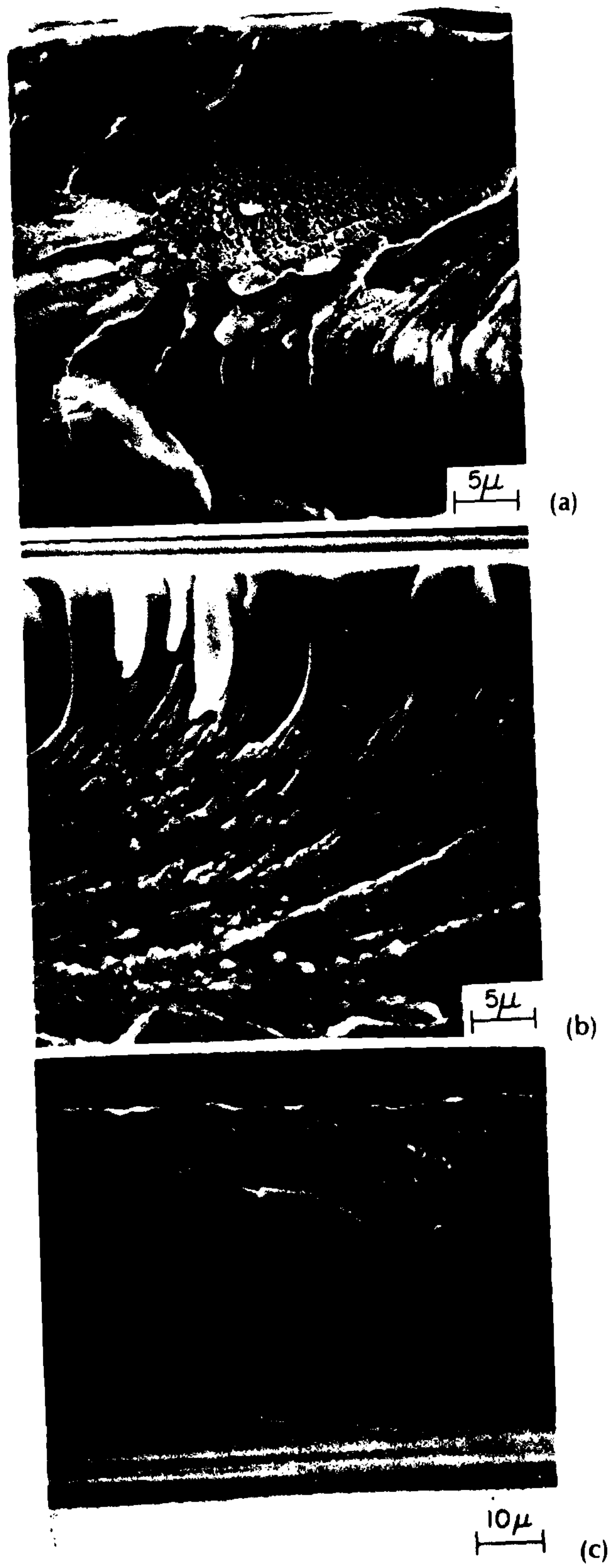

FIGURE 7. SEM PHOTOGRAPHS OF FRACTURE SURFACES OF $Fe_{32}Ni_{36}Cr_{14}P_{12}B_6$ IN THE FOLLOWING CONDITIONS: (a) AS CAST; (b) ANNEALED AT 300 C FOR ONE HOUR; (c) ANNEALED AT 375 C FOR ONE HOUR

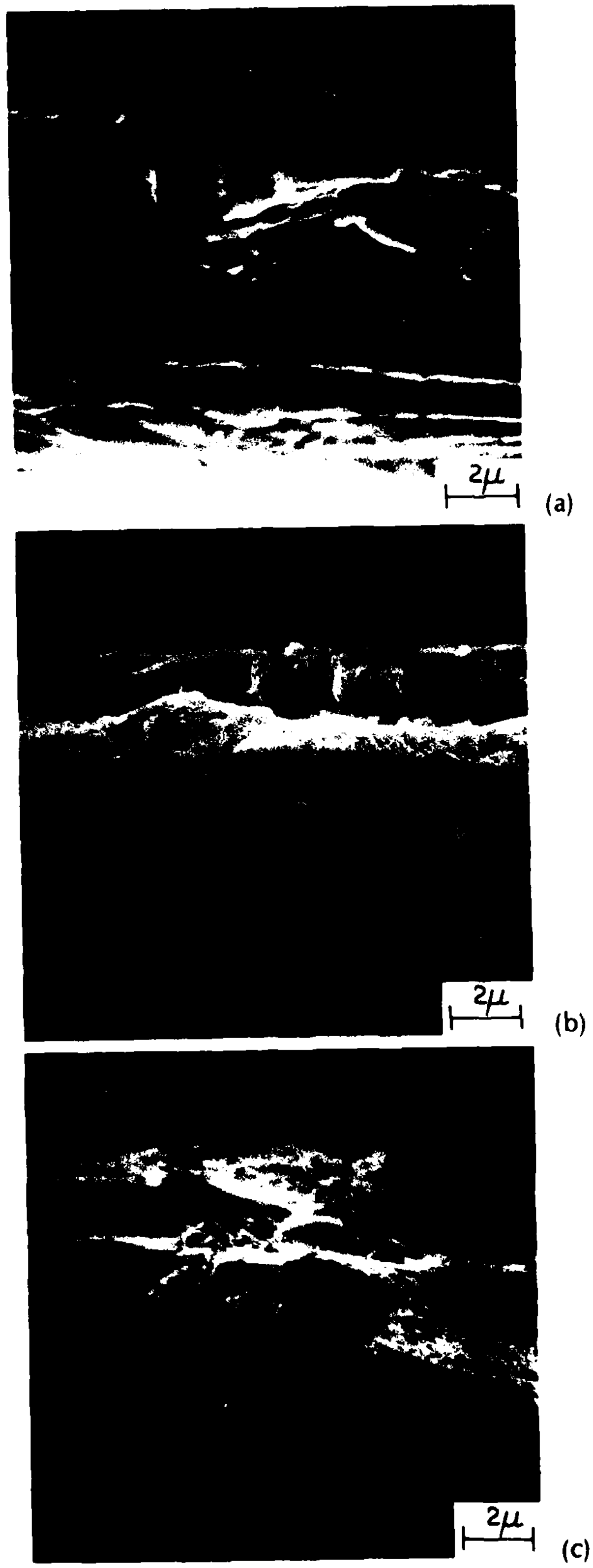

FIGURE 8. SEM PHOTOGRAPHS OF FRACTURE SURFACES OF $Fe_{32}Ni_{36}Cr_{14}Si_{6}B_{12}$ IN THE FOLLOWING CONDITIONS: (a) AS CAST; (b) ANNEALED AT 400 C FOR ONE HOUR; (c) ANNEALED AT 600 C FOR ONE HOUR

Microhardness Measurements

Vickers hardness versus annealing temperature is shown in Figure 9 for $Fe_{32}Ni_{36}Cr_{14}P_{12}B_6$ alloy. A sharp increase in microhardness occurred in the temperature range from 375 to 425 C. This transition temperature range is about 275 C higher than that in which ductility decreased sharply, as evident from Figure 3. The hardness reached a plateau range of about 1000 to 1050 at temperatures from 425 to 500 C; higher annealing temperatures were not investigated.

It was not possible to determine the Vickers hardness of alloy $Fe_{32}Ni_{36}Cr_{14}Si_6B_{12}$ because the melt spun filaments were too thin (~20 μm) and very narrow.

Corrosion Measurements

Tables 3 and 4 list the results of corrosion rate measurements obtained gravimetrically after exposing filaments in open beakers filled with 10 percent $FeCl_3$ solution. The $Fe_{32}Ni_{36}Cr_{14}P_{12}B_6$ alloy corroded at extremely low rates until annealed at 425 C, above which the corrosion rate (extrapolated to an annual rate) exceeded about 400 μm/year. $Fe_{32}Ni_{36}Cr_{14}Si_6B_{12}$ exhibited a higher corrosion rate in the as-cast state, namely, 140 μm/yr, but this rate decreased as a result of annealing in the temperature range from 22 to about 300 C. Anneals at 400 C and above resulted in rates that exceeded 240 μm/year, the upper limit of detectability for a specimen consumed in a 168-hour exposure period.

TABLE 3. CORROSION RATES OF $Fe_{32}Ni_{36}Cr_{14}P_{12}B_6$ IMMERSED IN 10% $FeCl_3$ SOLUTION AT 22 C FOR 168 HOURS

Annealing Treatment	Extrapolated Corrosion Rate, μm/yr
None (as cast)	0
100 C/1 Hour	0
200 C/1 Hour	0
300 C/1 Hour	0
375 C/1 Hour	0
425 C/1 Hour	368, 406
460 C/1 Hour	401, 423
500 C/1 Hour	415, 432

TABLE 4. CORROSION RATES OF $Fe_{31}Ni_{36}Cr_{14}Si_6B_{12}$ IMMERSED IN 10% $FeCl_3$ SDOLUTION AT 22 C FOR 168 HOURS

Annealing Treatment	Extrapolated Corrosion Rate, μm/yr
None (as cast)	140
100 C/1 Hour	39
200 C/1 Hour	8
300 C/1 Hour	85, 137
400 C/1 Hour	>240[a]
500 C/1 Hour	>240[a]
600 C/1 Hour	>240[a]

(a) Specimen partially disintegrated during the 168-hour exposure.

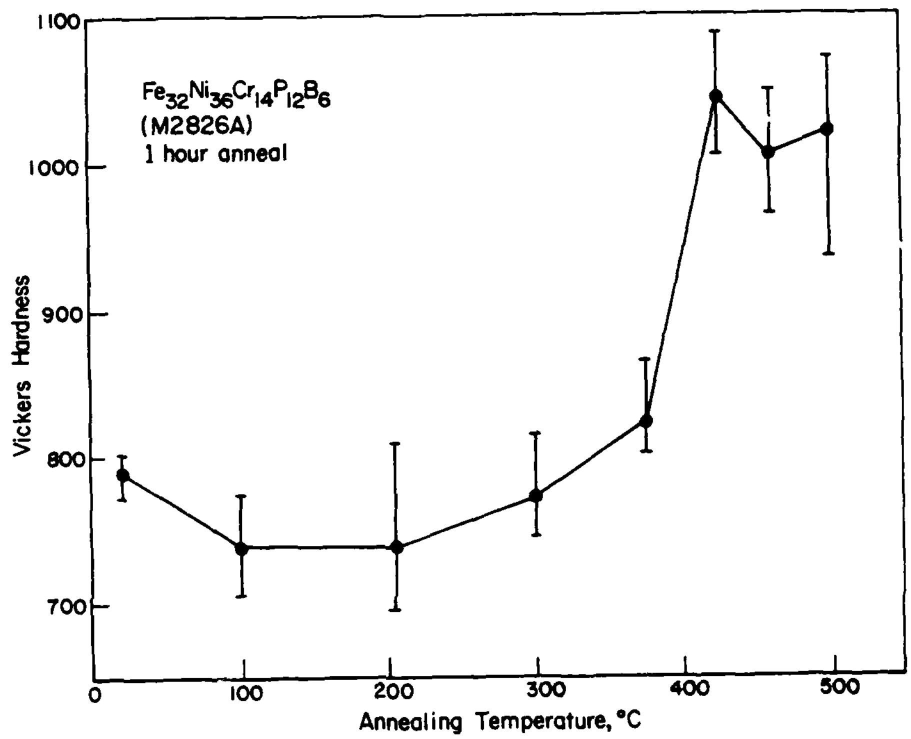

FIGURE 9. VICKERS HARDNESS VERSUS ANNEALING TEMPERATURE FOR $Fe_{32}Ni_{36}Cr_{14}P_{12}B_6$.

The influence of annealing on anodic polarization in NaCl electrolyte is shown in Figure 10 for $Fe_{32}Ni_{36}Cr_{14}P_{12}B_6$. The alloy was spontaneously passive in the as-cast state and after annealing at temperatures to 375 C, with a passive current density, i_p, of about 10^{-5} A/cm^2. Slight transpassive dissolution of chromium is evident at about -0.9 V(SCE), followed by secondary passivation and finally, pitting and oxygen evolution at potentials above 1.2 V(SCE). Annealing at 425 C and higher decreased the critical pitting potential, E_{cp}; annealing at 425 C produced an E_{cp} of 0.15 V(SCE), and at 460 C E_{cp} was 0.0 V(SCE). Alloys annealed at 425 C and above also exhibited several inflections in anodic current after the onset of pitting, suggestive of quasi-passivation of one phase within the alloy followed by dissolution of another phase at slightly higher potentials.

The ingot did not exhibit passivity over any potential range, but instead underwent active dissolution accompanied by copious pitting at all potentials.

A potential of 0.30 V(SCE) was arbitrarily selected as being in the passive potential range of polarization behavior, and the anodic current densities measured at this potential were plotted as a function of annealing temperature, Figure 11. Passivity appeared to be enhanced by annealing at 375 C, as suggested by the lower current density relative to that of the alloy; however, passivity was substantially degraded by annealing at 425 C and above.

$Fe_{32}Ni_{36}Cr_{14}P_{12}B_6$ exhibited spontaneous passivity in 1 M NaCl in the as cast condition, but it underwent pitting at potentials above 0.40 V(SCE), Figure 12. The passive current density was about $4 \cdot 10^{-6}$ A/cm^2. Annealing at 200 C introduced an active region between -0.50 and -0.33 V(SCE), followed by passivity in the current density range from 2 to $4 \cdot 10^{-6}$ A/cm^2. E_{cp} was not affected. However, annealing at 300 C and above decreased E_{cp} and increased i_p. The dependence of these variables on annealing temperature was not uniform; e.g., a 400 C anneal produced an i_p that exceeded that produced by 300 and 500 C anneals. The ingot underwent continuous active dissolution at all anodic potentials.

If 0 V(SCE) is selected as a typical passive potential for $Fe_{32}Ni_{36}Cr_{14}Si_6B_{12}$ and current densities at this potential are plotted in a manner analogous to Figure 11, then the behavior shown in Figure 13 becomes apparent. An increase in current density occurred at annealing temperatures above 200 C; at and below temperatures of 400 C the anodic current reflected passive corrosion, whereas at 500 C and above it was caused by pitting. The transition in current density versus annealing temperature was less rapid for $Fe_{32}Ni_{36}Cr_{14}Si_6B_{12}$ alloy than for $Fe_{32}Ni_{36}Cr_{14}P_{12}B_6$.

The induction times for pitting of $Fe_{32}Ni_{36}Cr_{14}P_{12}B_6$ in 1 M NaCl are shown in Figure 14. As cast filament and filaments annealed to 375 C did not experience sudden current increases, indicative of breakdown of passivity, during polarization for times exceeding 100 seconds. The breakdown times for alloys annealed at 425, 460, and 500 C were 9, 3, and <1 second, respectively. The current densities went through a maximum that was proportional to the annealing temperatures, but they never repassivated. Microscopic examination of the surfaces of the specimens polarized as shown by Figure 14 did not reveal any pits. Apparently, the localized attack giving rise to the high anodic current was on a submicron scale and resembled fine etching more than classical pitting corrosion.

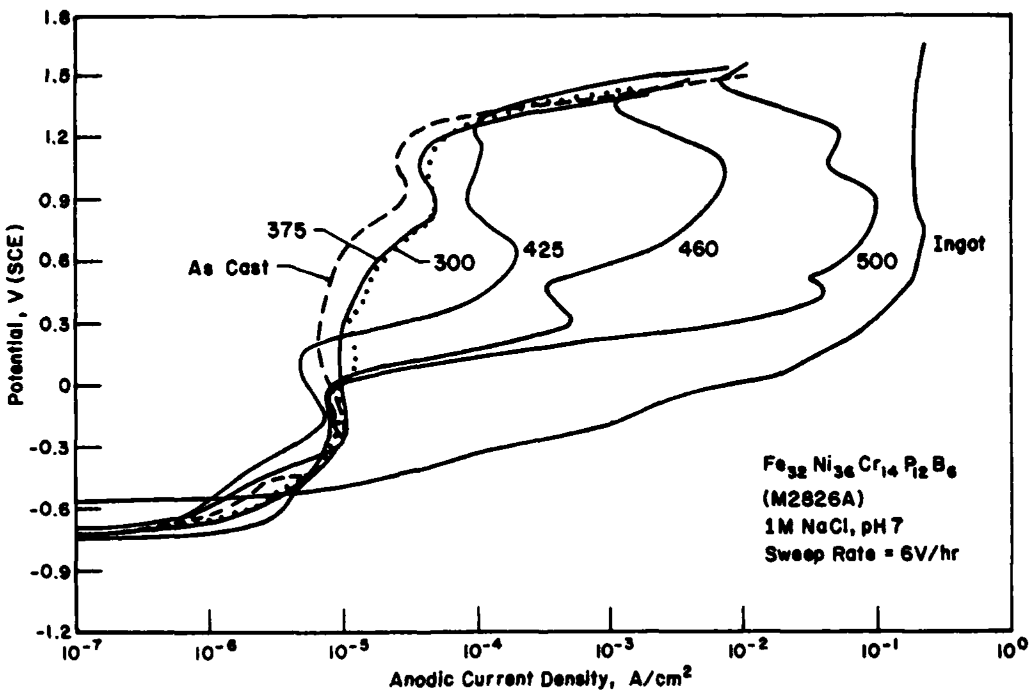

FIGURE 10. POTENTIAL VERSUS ANODIC CURRENT DENSITY FOR $Fe_{32}Ni_{36}Cr_{14}P_{12}B_6$ ANNEALED FOR ONE HOUR AT THE TEMPERATURES INDICATED, THEN POLARIZED IN 1 M NaCl AT pH 7

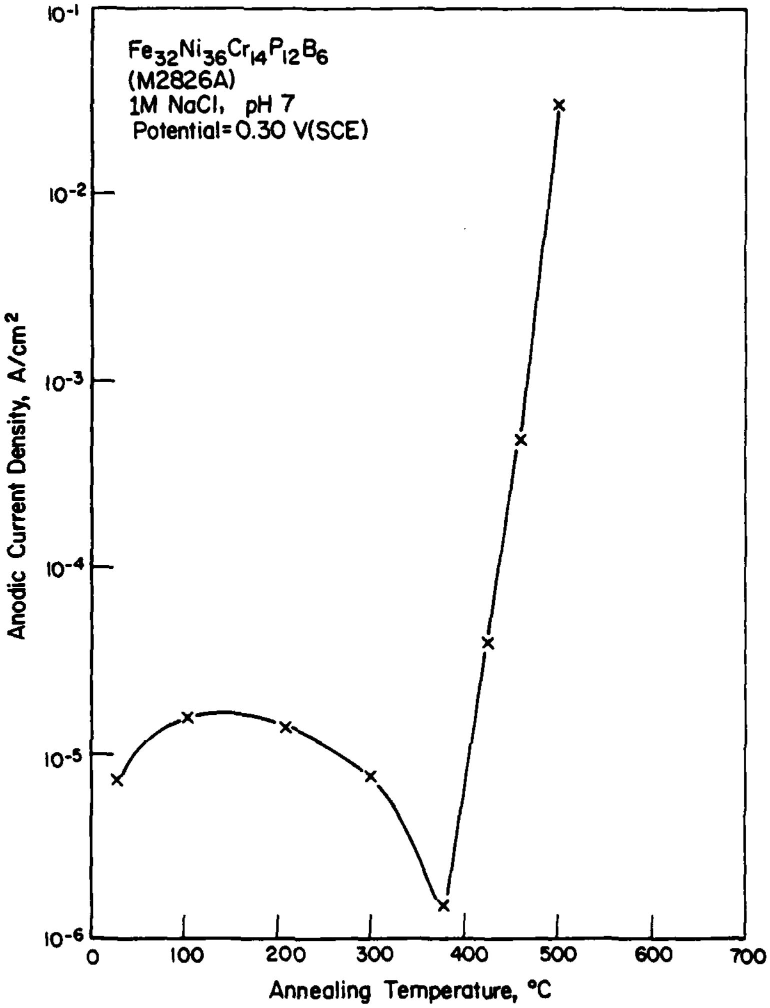

FIGURE 11. ANODIC CURRENT DENSITY AT 0.30 V(SCE) (FROM FIGURE 10) VERSUS ANNEALING TEMPERATURE FOR $Fe_{32}Ni_{36}Cr_{14}P_{12}B_6$

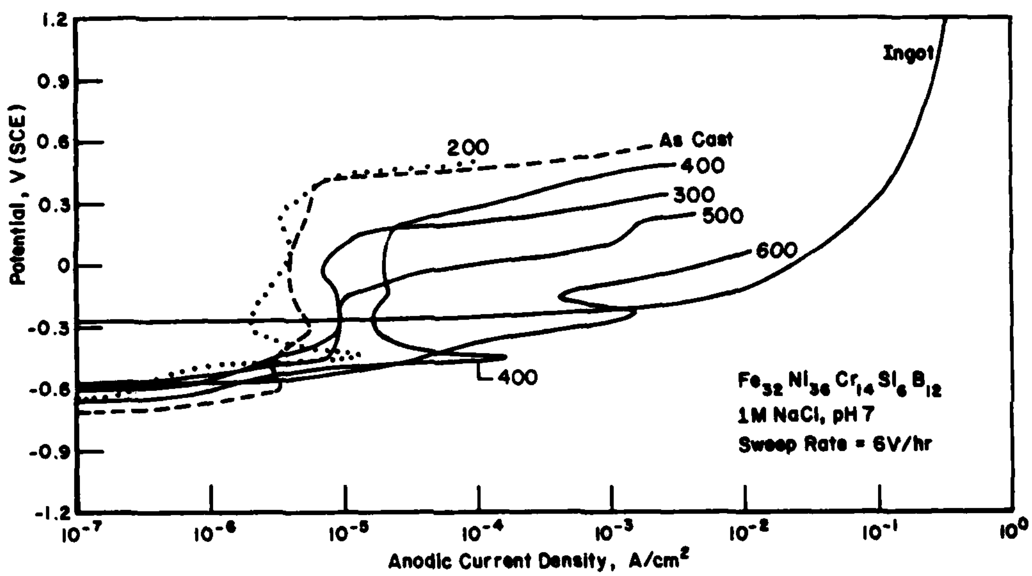

FIGURE 12. POTENTIAL VERSUS ANODIC CURRENT DENSITY FOR $Fe_{32}Ni_{36}Cr_{14}Si_6B_{12}$ ANNEALED FOR ONE HOUR AT THE TEMPERATURES INDICATED, THEN POLARIZED IN 1 M NaCl, pH 7

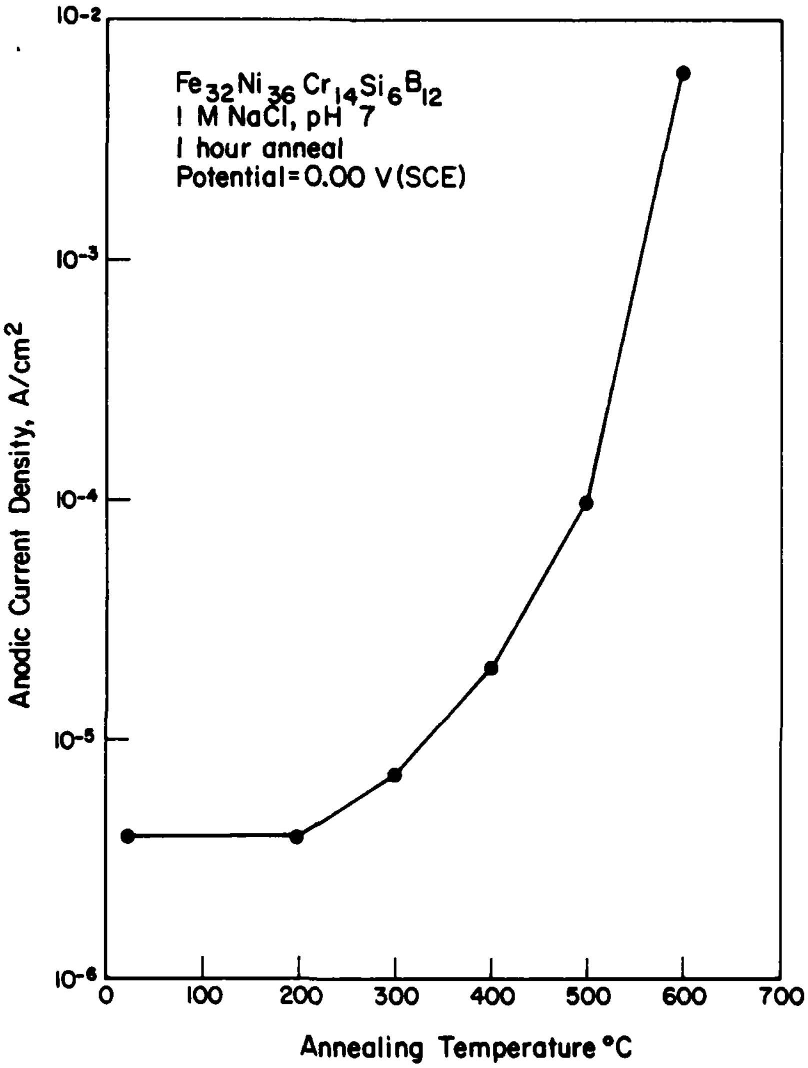

FIGURE 13. ANODIC CURRENT DENSITY AT 0.00 V(SCE) (FROM FIGURE 12) VERSUS ANNEALING TEMPERATURE FOR $Fe_{32}Ni_{36}Cr_{14}Si_6B_{12}$

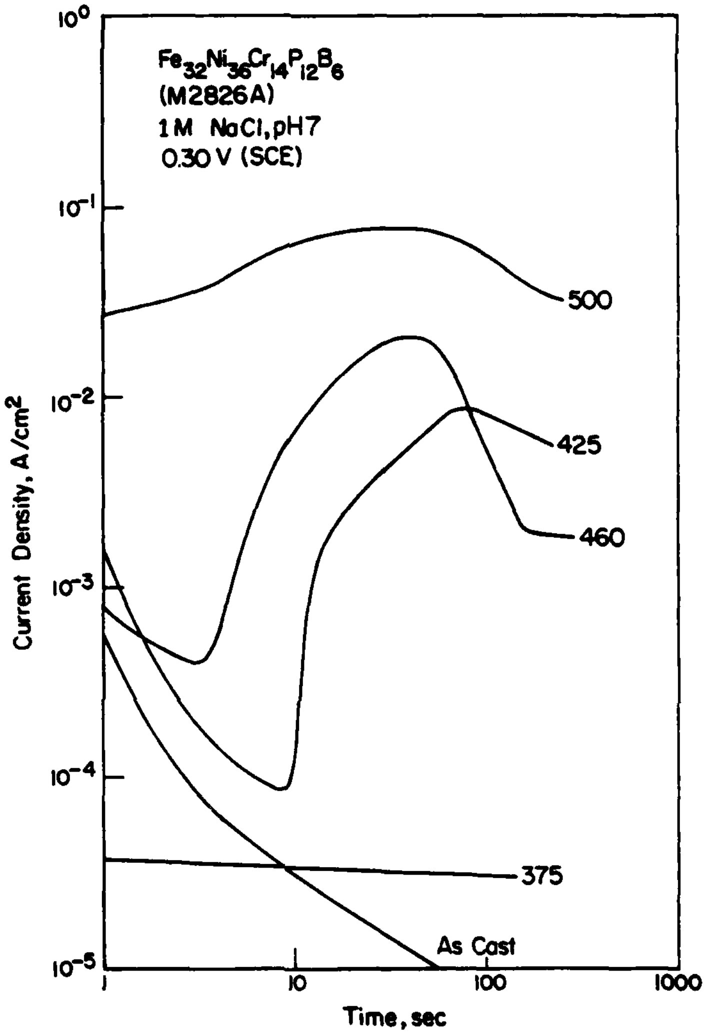

FIGURE 14. ANODIC CURRENT DENSITY VERSUS TIME OF POLARIZATION AT 0.30 V(SCE) IN 1 M NaCl, pH 7, FOR $Fe_{32}Ni_{36}Cr_{14}P_{12}B_6$

Annealing treatments were performed for one hour at the temperatures indicated.

DISCUSSION

Annealing (1979–1980 Research)

Data obtained by XRD and DSC verified that the $Fe_{32}Ni_{36}Cr_{14}P_{12}B_6$ alloy (commercial Metglas 2826 A) crystallized in a manner previously described.[13–15] The metastable crystalline phase MSI appeared at 400 C after one hour, but both MSI and a second metastable crystalline phase, MSII, were detected after annealing at 425 C and higher. However, when the P in this alloy was substituted by Si and B, as in $Fe_{32}Ni_{36}Cr_{14}Si_6B_{12}$, only MSI was detected, and this phase appeared between 400 and 500 C. It is not clear why the sputtered P-containing alloy, $Fe_{31}Ni_{30}Cr_{10}V_2P_{15}B_6$, showed only one transition peak (Table 2); this issue was not central to the study and hence, it was not pursued.

Comparison of Figures 1 and 3 indicates that embrittlement of $Fe_{32}Ni_{36}Cr_{14}P_{12}B_6$ preceded the onset of crystallization, as measured by XRD and DSC. The first crystalline phase to appear in this alloy, MSI, was detected at temperatures of 400 C and above, embrittlement, as characterized by a sharp decrease in fracture strain during bending, appeared at an annealing temperature between 100 and 200 C. This low temperature embrittlement is in qualitative agreement with the results of Luborsky and Walter[19], who demonstrated that the presence of phosphorus in amorphous metal-metalloid alloys causes embrittlement at temperatures as low as 100 C. Conversely, removal of phosphorus increased the embrittlement temperature to 225 C. As suggested by Pampillo[22], it is likely that the phosphorus segregated to heterogeneous sites within the filaments, such as voids formed during casting, and thereby provided an active path for brittle crack propagation during bending, as indicated by the presence of phosphorus on fracture surfaces of embrittled P-containing alloys.[18] The appearance of crystalline phases at temperatures above 400 C did not alter the relatively smooth decrease in γ_f with annealing temperature. This smooth transition in γ_f indicates that embrittlement was probably less affected by the appearance of crystalline phases than by phosphorus segregation preceding and accompanying crystallization.

It is not clear why filaments bent with the shiny (air-side) surface in tension showed higher ductility than those bent with the dull (wheel-side) surface in tension. One could logically expect the reverse to be true, because it has been shown that phosphorus enrichment occurs during casting near the shiny filament surface in $Fe_{40}Ni_{40}P_{14}B_6$, and to a depth exceeding 360 nm.[18] Since phosphorus promotes embrittlement, it might be expected that the shiny surface would have been more brittle. It is not known whether other effects, such as residual stresses resulting from the casting process, contributed to this difference in behavior between the two surfaces.

Removal of phosphorus from the alloy and substitution by Si and B yielded alloy $Fe_{32}Ni_{30}Cr_{14}Si_6B_{12}$. Phosphorus removal shifted the embrittlement temperature range to that coinciding with the appearance of MSI, which was detected after one hour anneals between 400 and 500 C. For this alloy the embrittlement reaction was not associated with segregation, but apparently it was caused by the appearance of a crystalline phase in the amorphous matrix. This phase appeared to be a NiFe solid solution similar to that observed in $Fe_{32}Ni_{36}Cr_{14}P_{12}B_6$.

The higher embrittlement temperature measured for $Fe_{31}Ni_{30}Cr_{16}V_2P_{15}B_6$, prepared at Battelle by melt spinning for earlier research[7-8], may have resulted from as-yet uncharacterized differences between quenching conditions. Such parameters as quench rate, filament thickness, wheel finish, and other factors may introduce structural and/or stress-related differences into strip that subsequently influence annealing response. Although the compositions of Metglas 2826A and the alloy prepared at Battelle were not identical, the similar phosphorus concentrations should have eliminated compositional differences as the sole cause of the difference in embrittlement behavior.

The embrittlement response to annealing was reflected in the fractography of $Fe_{32}Ni_{36}Cr_{14}P_{12}B_6$, Figure 7. Embrittlement of amorphous alloys has also been shown to be caused by annealing[22], hydrogen charging[23,24], and by hydrogen introduced by corrosion[25]. In all instances the vein-like pattern characteristic of the amorphous structure is gradually replaced by features resembling chevron or cleavage markings as embrittlement proceeds. Extremely brittle alloys exhibit fewer features and on a much smaller scale, indicative of the smaller degree of plastic flow accompanying fracture. Occasionally Wallner lines are observed on brittle fracture surfaces[25]; such features are characteristic of fracture of completely brittle solids, such as inorganic glasses and ceramics. No Wallner lines were found on fracture surfaces of materials examined during this research, perhaps suggesting that the degree of embrittlement was not sufficient to result in their formation during fracture.

Concerning $Fe_{32}Ni_{36}Cr_{14}Si_6B_{12}$ alloy, some ductility was evident on the fracture surface corresponding to a 400 C/1 hour anneal, Figure 8b. The fracture morphology corresponding to a 600 C/1 hour anneal was very rough, possibly indicating an intergranular component of fracture.

Unlike changes in fracture morphology, which paralleled embrittlement, microhardness was relatively unaffected by embrittlement. Stubicar[20] observed two hardness maxima for amorphous alloys, one in the amorphous temperature range and one at the crystallization temperature, about 400 C. However, in the present study a hardness maximum was observed only during crystallization, and it was undoubtedly caused by the appearance of MSI and/or MSII phases. It is proposed that analogous behavior would have been observed for the $Fe_{32}Ni_{36}Cr_{14}Si_6B_{12}$ alloy, had hardness measurements been possible, since $Fe_{80}Si_2B_{18}$ alloy has been shown to experience a hardness peak during crystallization.[20]

Examination of Tables 3 and 4 clearly shows that crystallization decreased the degree of passivity attained by the two alloys being investigated. Conversely, embrittlement exerted no detectable effect on corrosion behavior. The higher corrosion rate of $Fe_{32}Ni_{36}Cr_{14}Si_6B_{12}$ in the amorphous state can be attributed to the decrease of phosphorus which, when present, enhances incorporation of protective chromium oxyhydroxide in the passive films.[6] The increase in corrosion rate at 300 C for this alloy suggests either that compositional fluctuations immediately preceding crystallization can be important, or else that crystallization actually began at about 300 C but was not detected by XRD (see Figure 2) until a substantially higher annealing temperature was employed. The good agreement between Figures 2 and 4, relative to crystallization phenomena, suggests that structural and/or compositional changes that preceded crystallization were influential in decreasing the degree of passivity of the $Fe_{32}Ni_{36}Cr_{14}Si_6B_{12}$. Research with STEM would help to resolve the question of whether the decrease in corrosion resistance observed at 300 C, Table 4, is indeed a precrystallization phenomenon.

Anodic polarization verified the increase in anodic reactivity as a result of annealing. Figure 10 shows that the passive current density was not largely affected by crystallization, but rather, crystallization reduced the critical pitting potential, E_{cp}. The shift in E_{cp} was from about 1.2V (SCE) for a 375 C anneal to about 0 V(SCE) for a 500 C anneal, a total shift of 1.2 volts. As shown in Figure 11, at a typical passive potential of 0.30 V(SCE) a sharp increase in anodic current density occurred as a result of annealing at 425 C and higher. The transition in anodic current was more gradual for $Fe_{32}Ni_{36}Cr_{14}Si_{6}B_{12}$, as evident in Figure 14, and it began in the temperature range between 200 and 300 C. In this alloy the crystalline phase was exclusively MSI, and thus it must be concluded that formation of this phase is sufficient to reduce the integrity of the passive film developed during polarization. If MSI were deficient in chromium, as proposed[13], then it would be expected that its presence would constitute weak points (in the form of Cr-deficient regions) in the passive film that lead to easy electrochemical breakdown followed for pitting. The very small size of the precipitates, several tens of nm, prevented the verification of this hypothesis with, e.g., AES analysis of pitted regions; nevertheless, the appearance of chromium-deficient crystallites is proposed to account for the easy breakdown of passivity. The decreasing induction times for pit initiation shown in Figure 14 would be anticipated according to the hypothesis, and would form larger and better-developed crystallites for pit initiation at higher annealing temperatures.

Summary

Annealing of an amorphous alloy containing P and Cr below the crystallization temperature, T_c, resulted first in embrittlement, probably caused by segregation of phosphorus to internal defect sites. No evidence of crystallization was detected by conventional XRD, and no decrease in the passive nature of the alloy occurred. Annealing near T_c produced two metastable phases, which appeared to be face centered cubic NiFe solid solution (MSI) and a body centered tetragonal compound of the general composition $(Fe,Ni,Cr)_3$ (P,B). Crystallization was accompanied by a substantial decrease in corrosion resistance, presumably the result of introducing chromium-deficient flaws into the otherwise protective passive film. Removal of P from the alloy and substitution with Si and additional B eliminated embrittlement prior to the onset of crystallization. Crystallization decreased corrosion resistance for the same reason as for the P-containing alloy. Thus, crystallization and not low temperature segregation of phosphorus is necessary to decrease the corrosion resistance of this alloy class.

Localized Corrosion
(1977-1979 Research)

The results of earlier research concerning localized corrosion of amorphous alloys are documented in Appendices A, B, and C (References 9-11), as well as in References 7 and 8.

Summary of 1977–1979 Research

The primary reason for investigating crevice corrosion susceptibility of amorphous alloys was to differentiate between initiation-related and propagation-related corrosion behavior. It was reasoned that crevices would provide ready-made, or artificial sites for initiation of

localized attack, sites which do not exist on freely exposed amorphous alloy surfaces because of the very homogeneous nature of the alloy structure. Measurement of susceptibility to crevice corrosion would help to determine whether the corrosion resistance exhibited by these alloys extends to propagation as well as initiation phenomena.

Anodic potentiodynamic polarization curves showed that crevice corrosion should logically be expected to occur: the alloys exhibited enhanced corrosion at reduced electrolyte pH such as would be expected to develop during occluded cell corrosion, thus ensuring some degree of stability of active-passive cells on specimen surfaces. However, the very corrosive conditions that are required to produce corrosion of these alloys at sensible rates indicated that the degree of susceptibility to crevice corrosion would be considerably less than that of many crystalline steels of similar chromium content under similar exposure conditions. Subsequent experiments confirmed these predictions. Specifically, cold rolling of filaments produced a slight susceptibility to enhanced dissolution, presumably due to the formation of surface microcracks that initiated crevice corrosion. However, the depth of attack was only several μm when the crevices passivated.

More extensive experimentation, initially with a sandwich-type crevice cell and subsequently with an instrumented cell, verified that susceptibility of the chromium-containing amorphous alloys to crevice corrosion was indeed slight. Although classical crevice attack involving localized anodic dissolution and acidification of the anolyte could be made to occur, quite oxidizing (noble) potentials were required. These potentials were more than 1000 mV more noble for the 16 Cr amorphous alloy than for T304 stainless steel. Very interestingly, the potentials of amorphous crevice specimens did not decrease markedly after the onset of crevice corrosion, but rather they usually remained within several millivolts of the potential applied to the cathode. This behavior can be interpreted as a resistance to the loss of passivity, dissolution occurring instead *through* a passive film that prevailed relatively intact during crevice corrosion. This tendency of these alloys to remain covered by a passive layer is in contrast to the behavior of crystalline stainless steels, which experienced a loss of passivity that increased with time as corrosive conditions within the crevice became established. An indication of such a time-dependent activation is the large cathodic shift in electrode potential exhibited by T304 stainless steel.

The results of 1977–1979 research indicate that corrosion resistance of amorphous alloys used in this program extends to propagation as well as initiation phenomena. The alloys exhibited an apparent strong tendency to remain covered with a passive film, which other studies have shown to be analogous in structure and composition to the hydrated chromium oxyhydroxide found on conventional chromium-bearing steels. It is the ability of this film to exist under extremely corrosive conditions that confers excellent corrosion resistance. This ability, in turn, results presumably from the homogeneous nature of the alloys; that is, the absence of structural defects in the alloy matrices contributes to the integrity of the film. It is probable that the chemistry of the alloys also contributes to their excellent passivity. It has been claimed that the presence of phosphorus contributes to this enhanced passivity, and that it confers corrosion resistance by creating rapid anodic dissolution at unfilmed sites and thereby accelerating reformation of the film.[6] However, results presented recently by Wang and Merz[26] have shown that extremely corrosion resistant amorphous alloys can be prepared without any phosphorus, thereby demonstrating that phosphorus is not essential for corrosion resistance. The question of the role of phosphorus, and other metalloid additions, on conferring passivity should be the subject of future research.

It was also shown that sputtering can produce chromium-containing alloys that essentially are completely amorphous in structure. Physical properties of the sputtered alloys, such as degree of crystallinity, temperature of crystallization, and heat of crystallization closely resembled those of amorphous alloys of the same composition but prepared by liquid quenching, in this case melt spinning. The corrosion and electrochemical behavior of the sputtered deposits resembles, but is not identical to, that of melt spun alloys of the same composition. Specifically, the open circuit corrosion rates and the oxidation rates during anodic polarization of the sputtered deposits exceeded those of melt spun specimens, sometimes by about an order of magnitude. However, the sputtered deposits retained the same excellent resistance to pitting corrosion as their melt spun counterparts, with pitting occurring to a large degree only at potentials above about 1 V(SCE) in acidified chloride solutions. Thus, sputtering is a viable alternate technique for depositing amorphous Fe-Ni-Cr-P-B alloys while retaining their very good resistance to pitting corrosion.

CONCLUSIONS

Research on the effects of annealing of amorphous chromium-containing alloys has led to the following conclusions:

(1) $Fe_{32}Ni_{36}Cr_{14}P_{12}B_6$ is embrittled by annealing for one hour between 100 and 200 C, but crystallization does not occur below 400 C.

(2) The first phases to appear in this alloy are a NiFe solid solution and a phase of general composition $(Fe, Ni, Cr)_3 (P,B)$.

(3) $Fe_{32}Ni_{36}Cr_{14}Si_6B_{12}$ is embrittled by annealing above about 400 C, and this embrittlement coincides with crystallization of a NiFe phase from the amorphous matrix.

(4) Crystallization decreased corrosion resistance by reducing the critical pitting potential, presumably by introducing chromium-deficient sites in the otherwise protective passive film. Conversely, embrittlement in the absence of crystallization did not noticeably alter corrosion behavior.

Research during 1977-1979 resulted in the following conclusions:

(1) The amorphous chromium-containing alloys that were studied satisfy two primary requirements for susceptibility to crevice corrosion and to O.C.C. in general; they exhibit active-passive transitions in certain corrodents, and their corrosion rates increase with decreasing pH.

(2) The alloys undergo crevice corrosion in prepared crevices, but only at relatively noble applied potentials exceeding about 1 V(SCE) for the higher Cr alloys.

(3) Although acidification of anolyte pH occurs during crevice corrosion, activation of the potential of the anode is slight. This behavior indicates that a fairly protective film may be present even during crevice attack.

(4) As evaluated in crevice and test cells, crevice corrosion resistance of amorphous alloys containing from 2 to 16 atomic percent Cr greatly exceeds that of T304 stainless steel.

(5) Cold rolling of amorphous alloys reduces the initiation potential for crevice corrosion to values near the free corrosion potential. This phenomenon is ascribed to the formation of surface microcracks, after Devine.[12] However, during growth, the crevices widen, passivate, and cease to propagate.

(6) Increasing the chromium content in the alloys substantially increases their resistance to crevice corrosion.

(7) Sputtering can be used to deposit chromium-containing alloys that display amorphous structures quite similar to those of alloys prepared by melt spinning.

(8) The corrosion resistance of sputtered specimens is somewhat less than that of melt spun specimens of similar compositions, regarding open circuit corrosion rates and dissolution during anodic polarization.

(9) The resistance to pitting of sputtered alloys is essentially the same as that of melt spun alloys of similar composition. Pitting corrosion occurs rapidly in acidified chloride electrolytes only at potentials above about 1 V(SCE).

Thus, amorphous chromium-containing alloys exhibit considerable resistance to corrosion under conditions favoring easy initiation, namely, in prepared crevices. It must be concluded that their corrosion resistance is not simply the result of difficulty in initiating localized dissolution, but that it results in large part from the ability of the alloys to *maintain* passivity under extremely aggressive conditions.

REFERENCES

1. Naka, M., Hashimoto, K., and Masumoto, T., "High Corrosion Resistance of Chromium-Bearing Amorphous Iron Alloys in Neutral and Acidic Solutions Containing Chloride", Corr., **32** (4), 146 (1976).

2. Diegle, R., and Slater, J., "Influence of Crystallinity on Corrosion Behavior of Ferrous Alloys", Corr., **32** (4), 155 (1976).

3. Hashimoto, K., and Masumoto, T., "Extremely High Corrosion Resistance of Chromium-Containing Amorphous Iron Alloys", *Rapidly Quenched Metals,* Procs., Second Int. Conf. on Rapidly Quenched Metals (1975), Edited by N. J. Grant and B. C. Giessen, p. 285.

4. Hasimoto, K., Asami, K., Masumoto, T., and Shimodaira, S., "Characteristics of Passivity of Extremely Corrosion-Resistant Amorphous Iron Alloys", Corr. Sci., **16** (2), 71 (1976).

5. Asami, K., Hashimoto, K., Masumoto, T., and Shimodaira, S., "ESCA Study of the Passive Film on an Extremely Corrosion-Resistant Amorphous Iron Alloy", Corr. Sci., **16** (12), 909 (1976.)

6. Hashimoto, K., Naka, M., Asami, K., and Masumoto, T., "XPS and Electrochemical Studies of Effects of Metalloid Additives on Corrosion Behavior of Amorphous Iron-Chromium Alloys", Corrosion Engineering (Boshoku Gijutsu), **27**, 279 (1978).

7. Diegle, R. B., and Lineman, D. M., "Investigating Localized Corrosion and Sputtering Feasibility of Amorphous Chromium-Containing Alloys", Interim Technical Report No. ONR-00014-77-C-0488 to Office of Naval Research, April, 1978.

8. Diegle, R. B., and Lineman, D. M., "Investigating Localized Corrosion and Sputtering Feasibility of Amorphous Chromium-Containing Alloys", Interim Technical Report No. ONR-00014-77-C-0488-2 to Office of Naval Research, May, 1979.

9. Diegle, R. B., "Localized Corrosion of Amorphous Fe-Ni-Cr-P-B Alloys", Corr., **35** (6), 250 (1979).

10. Diegle, R. B., "Crevice Corrosion of Glassy Fe-Ni-Cr-P-B Alloys", Corr., **36** (7), 362 (1980).

11. Diegle, R. B., and Merz, M. D., "Corrosion Behavior of Glassy Chromium-Containing Alloys Prepared By Sputtering", J. Electrochem. Soc., **127** (9), 2030 (1980).

12. Devine, T. M., "Anodic Polarization and Localized Corrosion Behavior of Amorphous $Ni_{35}Fe_{30}Cr_{15}P_{14}B_6$ in Near-Neutral and Acidic Chloride Solutions", J. Electrochem. Soc., **124** (17), 38 (1977).

13. Naka, M., Hashimoto, K., and Masumoto, T., "Effect of Heat Treatment on Corrosion Behavior of Amorphous Fe-Cr-P-C and Fe-Ni-Cr-P-B Alloys in 1 N HCl", to be published.

14. von Heimendahl, M., and Maussner, G., "The Metastable Crystallization Phases in the Amorphous Alloy Metglas 2826 A", J. Mat. Sci., **14**, 1238 (1979).

15. von Heimendahl, M, and Maussner, G., "Kinetics of Crystallization Studied by T.E.M. in Metglas 2826 A ($Fe_{32}Ni_{36}Cr_{14}P_{12}B_6$)", *Proc.*, Third Int. Conf. on Rapidly Quenched Metals, The Metals Society, London (1978), Volume 1, p. 424.

16. Walter, J. L., and Bartram, S. F., "Crystallization of Some Amorphous Alloys, " ibid., p. 307.

17. Turn, J. C., Jr., and Latanision, R. M., "Mechanisms of Corrosion of Glassy Copper Zirconium Alloys", Seventh Int. Conf. on Metallic Corrosion, Rio de Janeiro, Brazil, October 4-11, 1978.

18. Walter, J. L., Bacon, F., and Luborsky, F. E., "An Auger Analysis of the Embrittlement of the Amorphous Alloy $Ni_{40}Fe_{40}P_{14}B_6$", Mat. Sci. Eng., **24**, 239 (1976).

19. Luborsky, F. E., and Walter, J. L., "Stability of Amorphous Metallic Alloys", J. Appl. Phys., **47** (8), 3648 (1976).

20. Stubicar, M., "Microhardness Characterization Stability of Fe-Ni-Base Metallic Glasses", J. Mat. Sci., **14**, 1245 (1979).

21. Kawashima, A., Hashimoto, K., and Masumoto, T., "Fractographic Study of Amorphous Iron-Base Alloys Embrittled by Hydrogen and Heat-Treatment", Scr. Met., **14**, 41 (1980).

22. Pampillo, C. A., "Annealing Embrittlement in an Iron-Nickel-Based Metallic Glass", Mat. Sci. Eng., **33**, 275 (1978).

23. Kawashima, A., Hashimoto, K., and Masumoto, T., "Stress Corrosion Cracking of Amorphous Iron Base Alloys", Corr. Sci., **16** (12), 935 (1976).

24. Viswanadham, R. K., Green, J.A.S., and Montague, W. G., Scr. Met., **10**, 229 (1976).

25. Kawashima, A., Hashimoto, K., and Masumoto, T., "Hydrogen Embrittlement of Amorphous Fe-Cr-Mo Alloys", Corr., **36** (10), 577 (1980).

26. Wang, R., and Merz, M. D., "Corrosion Resistant Amorphous Stainless Steels Containing Tungsten", Abstract Number 54, The Electrochemical Society, May 6-11, 1979.

APPENDIX A

LOCALIZED CORROSION OF AMORPHOUS Fe-Ni-Cr-P-B ALLOYS

Localized Corrosion of Amorphous Fe-Ni-Cr-P-B Alloys*

*RONALD B. DIEGLE**

Abstract

Experiments were performed with a series of amorphous Fe-Ni-Cr-P-B alloys of varying Cr content to characterize their susceptibility to crevice corrosion. Potentiodynamic and potentiostatic polarization of freely exposed specimens was performed in simulated crevice solutions (1M NaCl at pH 1-7, and 6% $FeCl_3$ at pH 1.4). Crevice corrosion experiments were conducted in an artificial crevice cell. Polarization in the simulated crevice electrolytes indicated that alloys containing 2 to 16 At.% Cr can passivate in even 1M NaCl, pH 1, and they do not experience significant pitting at potentials active to that at which oxygen evolution occurs. In agreement with previously published results,[1] only a few At.% Cr were needed to confer passivity; even the alloy containing 2% Cr achieved a passive current density of only 10^{-1} A/m^2 in 1M NaCl at pH 1, and it did not pit below about 1.20 V(SCE). Results indicated, however, that the alloys meet certain requirements for susceptibility to crevice corrosion and occluded cell corrosion in general; that is, they passivate at sufficiently anodic potentials, and the intensity of active dissolution increases with decreasing pH. The amorphous alloys were considerably more inert to corrosion than T304 and Incoloy 800 steels, suggesting a lesser susceptibility to crevice attack. Experiments with the artificial crevice cell confirmed that the amorphous alloys can indeed be forced to crevice corrode, but only at very anodic (transpassive) potentials. They are considerably more resistant to crevice attack than the crystalline Cr-containing alloys.

A major reason for the initial interest in the corrosion behavior of amorphous Cr containing alloys derived from the fact that their composition is similar to that of crystalline stainless alloys, *i.e.*, both alloy classes contain Fe, Ni, and Cr. Thus, the simultaneous presence of these three metal components provided, for the first time, an opportunity for studying corrosion of a stainless type alloy composition in the absence of crystalline defects. Early studies showed that amorphous alloys of the general compositions Fe-Ni-Cr-P-B and Fe-Ni-Cr-P-C are very corrosion resistant, especially with respect to pitting corrosion.[1-4]

Potentiodynamic polarization techniques in neutral and acidified chloride solutions demonstrated that the critical pitting potential (E_{cp}) of these amorphous alloys is several tenths of a volt more noble than that of many conventional stainless steels of similar or greater Cr content. One group of researchers showed that the minimum amount of Cr needed to confer passivity was only 8 At.%,[1] in contrast to the approximate 12 At.% required in crystalline stainless steels. Thus, preliminary studies of this new class of materials indicated that it constitutes a novel alloy system with not only improved corrosion resistance relative to crystalline stainless steels, but also with the potential for conserving Cr, a critical resource.

The favored hypothesis to explain the good pitting resistance of amorphous Cr containing alloys is based on their homogeneous structure. Because the alloys are amorphous, they are free of grain boundaries, dislocations, stacking faults, and other defects associated with the crystalline state. Because they are quenched at rates in excess of 10^5 K/s, they are also free of severe microsegregation and second phases, which are formed by solid state diffusion. At most, they are somewhat heterogeneous on an atomic scale because of short range ordering and clustering. The alloys, therefore, are presumed to resist pitting because of the difficulty of *initiating* localized attack. The fact that heterogeneous surface sites, at which pitting often initiates in crystalline alloys, are absent in amorphous alloys is used to rationalize the fact that E_{cp} is considerably more

*Submitted for publication June, 1978; revised November, 1978.
*Battelle Columbus Laboratories, Columbus, Ohio.

Reprinted from CORROSION, Vol. 35, No. 6, pp. 250-258 (1979) June

TABLE 1 – Effect of O_2 on Open Circuit Corrosion Rates in 1N H_2SO_4 + 1M NaCl[1]

Alloy	Crystalline State	O_2 Available	Corrosion Rate (mpy)
Metglas 2826A	Amorphous	Yes	<0.00:
Metglas 2826A	Amorphous	No	3.0, 3.0
T304	Crystalline	Yes	21.5
T304	Crystalline	No	5.6, 7.0

(1)Results of previous unpublished research by the author.

noble than in crystalline alloys. That the passive films formed on amorphous Fe-Ni-Cr-P-C alloys are not unique, but closely resemble those on crystalline stainless steels with respect to composition and structure,[5] supports th hypothesis that structural differences between the alloys and not between the passive films account for the different degrees of corrosion resistance.

Therefore, the key to the resistance of certain amorphous alloys to pitting appears to result from the difficulty of pit initiation, but not necessarily from a resistance to propagation. It stands to reason that if pits can be initiated, they might propagate re ily. Indeed, Devine demonstrated this fact by promoting localized corrosion in Metglas 2826A (Allied Chemical's $Fe_{30}Ni_{36}Cr_{14}P_{14}B_6$ alloy) by first cold rolling it to induce surface microcracks.[6] Local ed attack occurred in the cracked specimen at a potential which was well active to that required for the undeformed alloy. It presumably resulted because of easy initiation at microcracks produced by rolling.

It was also demonstrated that the open circuit corrosion rate of Metglas 2826A in an acidified chloride solut n sealed from oxygen is nearly 1000 times greater than that for specimens in the same solution open to the atmosphere, as shown in Table 1.[7] Therefore, it appears that oxygen is necessary to promote passivity of the amorphous alloys, just as it is for conventional Cr bearing stainless steels.

The above observations were interpreted as indicating a possible Achilles heel in the otherwise remarkable c sion resistance of these alloys; namely, they might be highly susceptible to crevice corrosion. Because crevice corrosion does not require surface heterogeneities for initiation, and because oxygen depletion can readily occur within crevices, it was wondered whether the alloys might readily corrode in a crevice geometry, unlike their performance when evaluated in a freely exposed geometry. The research described in this paper sought to determine the degree to which amorphous Cr containing alloys, which otherwise resist localized corrosion remarkably well, are susceptible to crevice corrosion. A second purpose of this study was to determine the amount of Cr needed to confer resistance to crevice attack.

Experimental Procedure

Materials

Five amorphous alloy compositions were prepared at Battelle for this research program. The Cr concentration was varied from 2 to 16 At.% to determine the amount of Cr needed to confer corrosion resistance under the exposure conditions used. The compositions of these alloys are presented in Table 2. The alloy from Allied Chemical Corporation was included as representative of an amorphous alloy of composition similar to the 16 At.% Cr Battelle alloy, but produced at another laboratory. T304 stainless was included as an example of commercial stainless steels. Incoloy 800 was evaluated because the Fe, Ni, and Cr levels approximate those in the 16 At.% Battelle alloy, but they are present in a crystalline rather than amorphous structure.

The five Battelle alloys were first cast into pancake shaped ingots by conventional casting techniques involving induction melting of pure components in a controlled atmosphere. Next, 30 gram portions from each crystalline ingot were removed and melt spun into amorphous filaments. The melt spinning was performed as shown schematically in Figure 1. The liquid impinged on a water cooled copper wheel rotating at 2550 m/minute in argon. The resulting filaments were about 800 μm wide and 30 μm thick.

The filaments were evaluated by differential scanning calorimetry (DSC) as a means of assessing the presence of an amorphous structure. The heating rate was 5 C per minute.

Electrochemical Techniques

A variety of electrochemical techniques were used to evaluate the various alloys. A specimen holder was specially adapted to the filament specimen geometry by soldering a 2 cm length of filament to a fine copper wire extending through a glass tube. The opper and solder were masked with an acid resistant lacquer which also served to seal the lower end of the tube. Polarization, both potentiostatic and potentiodynamic, was performed in a glass cell of about 1 liter capacity equipped with Luggin capillary, counter electrodes separated from the bulk electrolyte by porous glass frits, and a fritted bubbler for deaeration with tank nitrogen. Polarization was accomplished with an electronic potentiostat and electronic function generator. Potential scans were performed by sweeping the potential from the open circuit potential to various anodic values. All potentials were measured relative to a saturated calomel electrode (SCE) that was external to the cell. Specimen surfaces were first prepared by cathodic polarization to -1.5 V (SCE) for up to 2 minutes to achieve an active and quasistationary open circuit potential. Except in the study of simulated crevice corrosion, the electrolytes were deaerated by vigorously bubbling nitrogen through

TABLE 2 – Compositions of Alloys Used in Corrosion Studies

Preparation Technique	Source	Amorphous	Composition, At.%[1] Fe	Ni	Cr	P	B	Si	C	Mn	Ti	Al
Melt Spinning	Battelle	Yes	47	30	2	15	6					
		Yes	44	30	5	15	6					
		Yes	42	30	7	15	6					
		Yes	39	30	10	15	6					
		Yes	33	30	16	15	6					
Melt Spinning	Allied	Yes	32	36	14	12	6					
Conventional casting and rolling	Mill	No	69	8	20			1.2	0.00	1.7		T304 stainless steel
		No	46	31	22				0.00		0.005	0.008 (Incoloy 800)

(1)Compositions of T304 and Incoloy 300 are nominal.

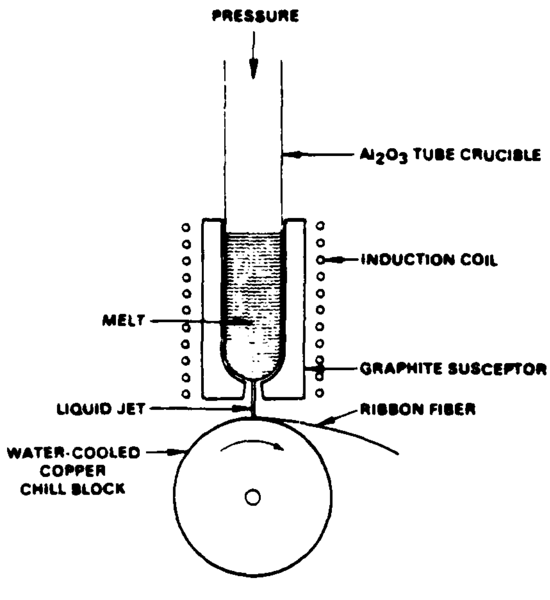

FIGURE 1 – Schematic diagram of the melt spinning apparatus used to produce certain alloys studied in this program.

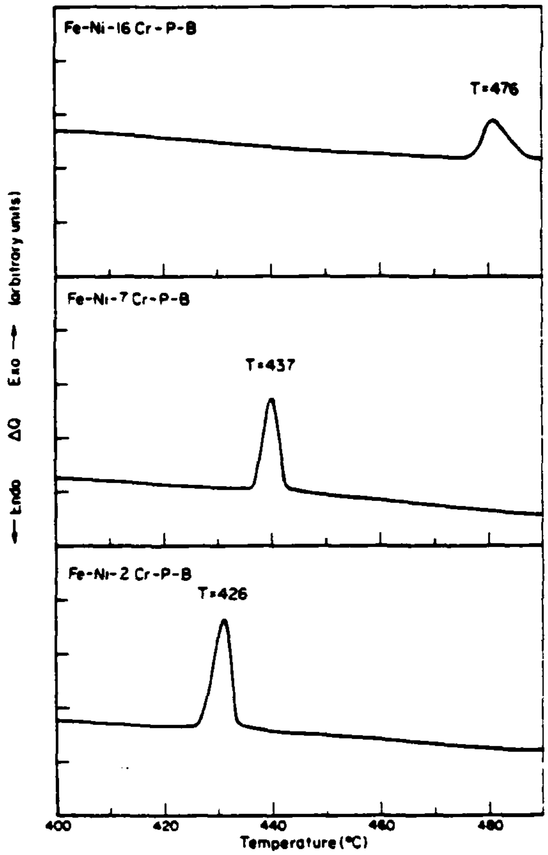

FIGURE 3 – Differential scanning calorimetry (DSC) curves for melt spun alloys with the indicated Cr contents. Scan rate was 5 C/minute.

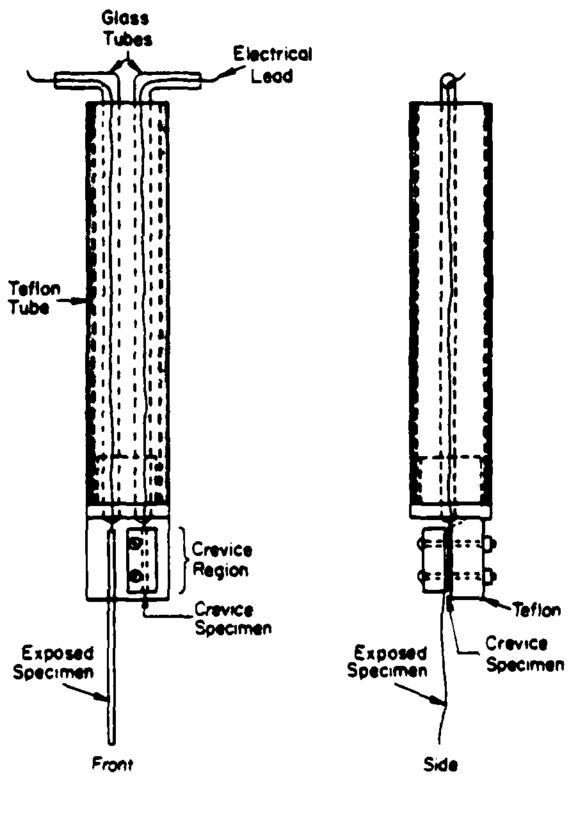

FIGURE 2 – Schematic diagram of the PTFE crevice cell used to evaluate crevice corrosion susceptibility.

them prior to each experiment. Two scans, in independent experiments, were performed for nearly all alloy-corrodent combinations studied.

The pH of the various chloride solutions used throughout the research was carefully adjusted prior to each experiment. Adjustment was made with HCl or NaOH, and the pH was periodically checked with a pH electrode previously calibrated in appropriate buffer solutions.

Several crevice cell designs were tried for evaluating susceptibility to crevice corrosion. The one chosen for this research is shown schematically in Figure 2. The crevice was formed by clamping the specimen between two pieces of PTFE. The total specimen area within the crevice was about 0.2 cm^2; no special surface pretreatment was used. A specimen of total surface area ten times greater than that within the crevice served as the external (cathode) specimen. In practice, the two electrodes (crevice and external) were electrically connected to each other through a zero resistance ammeter (ZRA). This crevice electrode assembly was made the working electrode of an electrochemical cell. The external electrode was polarized potentiostatically to a specific potential, and the resulting current flowing between crevice and external specimens (as read on the ZRA) was recorded over a specific period. This procedure enabled determination of (a) whether crevice corrosion occurred, (b) the critical potential for initiation, E_{cc}, (c) the time required for its initiation; and (d) severity of attack, as measured by the steady state cell current. The cell thus enabled measurement of crevice corrosion in real time for the nonideal geometry of melt spun filaments.

A-4

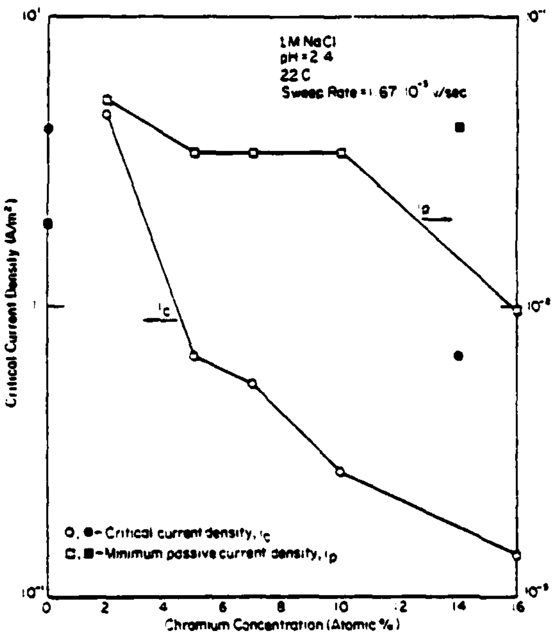

FIGURE 4 – Critical and passive current densities versus Cr content for amorphous alloys polarized in 1M NaCl, pH 2.4. Open symbols refer to alloys produced at Battelle and solid symbols refer to Metglas 2826 and 2826A.

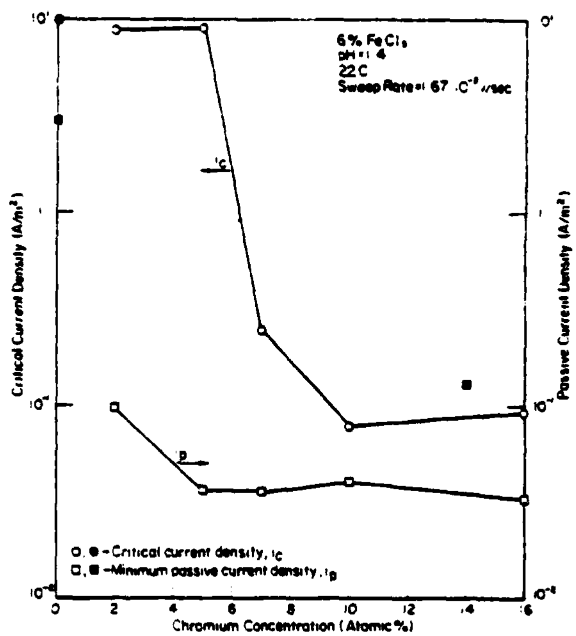

FIGURE 5 – Critical and passive current densities versus Cr content for amorphous alloys polarized in 6% $FeCl_3$, pH 1.4. (See Figure 4 for explanation of symbols.)

Results and Discussion

Structural Characterization of Melt Spun Alloys

Three of the five alloy compositions were evaluated by DSC to determine whether they were amorphous.[(1)] Results of these DSC scans are shown in Figure 3. The alloys exhibited sharp, narrow peaks characteristic of crystallization of metallic glasses as reported by other workers.[8] The measured crystallization temperatures were: 2 Cr, 426 C, 7 Cr, 437 C, and 16 Cr, 476 C. These temperatures are within the 400 to 500 C temperature range in which amorphous Fe-Ni-Cr-P-B alloys are known to crystallize. Therefore, it is concluded that the alloys produced at Battelle by melt spinning exhibited predominantly amorphous behavior.

Polarization in Simulated Crevice Solutions

Behavior of the amorphous and crystalline alloys in simulated crevice solutions was characterized extensively by potentiodynamic and potentiostatic polarization. These experiments were performed to predict: (1) whether crevice corrosion should logically be expected to occur, (2) whether it should be severe or slight relative to crevice corrosion of crystalline alloys, and (3) the degree to which increasing the Cr content could be expected to ameliorate the severity of attack encountered in actual crevices.

Data from a series of polarization curves are condensed and presented in Figures 4 and 5. These figures show the dependences of the critical current density required to initiate passivity (i_c) and the minimum passive current density (i_p) on Cr content for two chloride solutions. In Figure 4, it is evident that i_c was decreased by a factor of 30 and i_p by a factor of 5 when Cr was increased from 2 to 16 At.%. In Figure 5, i_c and i_p were decreased by factors of 92 and 3, respectively, over the same Cr range. Several features of this polarization behavior are noteworthy:

1. The degree of passivity achieved by the 2 Cr alloy was remarkably good (0.05 and 0.097 A/m^2) considering the extremely corrosive nature of these two electrolytes.

2. The effect of increasing the Cr content was much stronger on facilitating passivation than on enhancing the degree of passivity ultimately reached.

3. Although it is not evident in these figures, these alloys did not exhibit localized corrosion attack[(2)] at potentials below that required for oxygen evolution, which was about 1 V (SCE) and above.

4. The Metglas 2826A alloy exhibited deviations in i_c and i_p generally by factors of 10 or less relative to the curves plotted with the BCL alloys. Metglas 2826A displayed higher corrosion rates, even though it contained more Ni and less Fe than the in-house alloys.

Paralleling the second observation above, the effect of Cr in crystalline alloys has also been observed to decrease i_c by a greater degree than i_p.[9] Apparently, Cr was needed to enhance protection of films formed at potentials corresponding to active dissolution of the Fe-Ni-P-B alloy, because at these potentials, the oxidation products of iron are more soluble than those of Cr.[10] At more noble potentials corresponding to passivity of Fe-Ni-P-B, the role of Cr was less significant because iron was able to develop a fairly protective passive film by itself. Here, the effect of Cr was to enhance the protection provided by the passivating iron rich layer.

The above data can be used to predict several features concerning crevice and other forms of localized corrosion of these amorphous alloys. For localized corrosion or occluded cell corrosion (OCC) to occur, an alloy must exhibit two features regarding polarization behavior. First, it must be able to passivate in the electrolyte of interest. Second, increasing the chloride level and/or decreasing the pH should accelerate the rate of attack. This type of behavior insures stability of active-passive cells on the alloy surface.

---

(1) The term "amorphous" is used here to refer to materials that do not possess crystallinity which is detectable by straightforward techniques such as DSC, selected area electron diffraction, and X-ray diffraction.

(2) Intense scrutiny by SEM revealed an occasional pit which grew to less than about 10 μm in depth, and then apparently stopped growing and passivated.

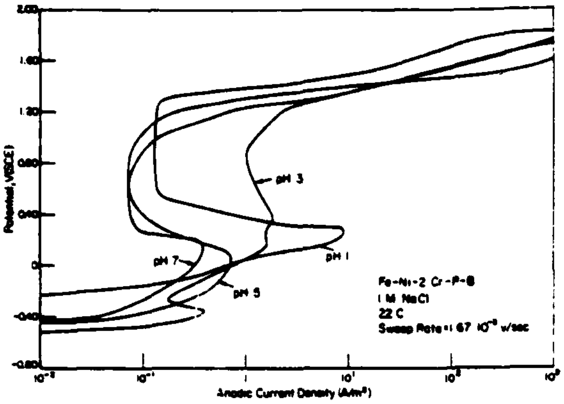

FIGURE 6 – Potentiodynamic polarization curves for the 2 At.% Cr amorphous alloy in 1M NaCl adjusted to several pH values.

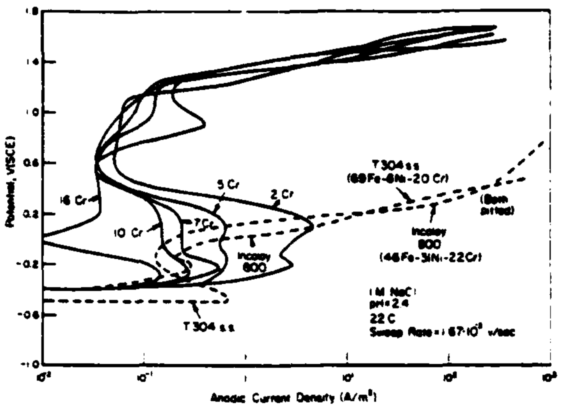

FIGURE 9 – Potentiodynamic polarization curves for amorphous melt spun alloys of the indicated Cr contents, and for crystalline T304 and Incoloy 800 alloys.

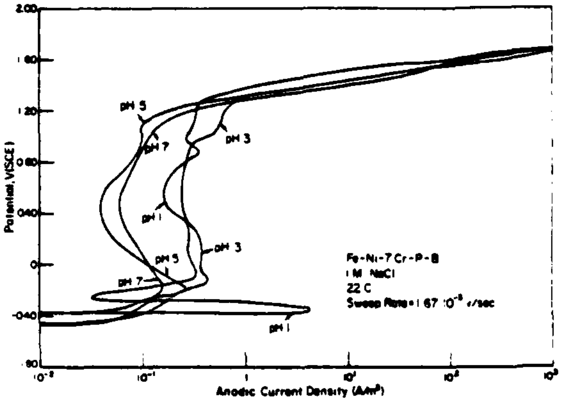

FIGURE 7 – Potentiodynamic polarization curves for the 7 At.% Cr amorphous alloy in 1M NaCl adjusted to several pH values.

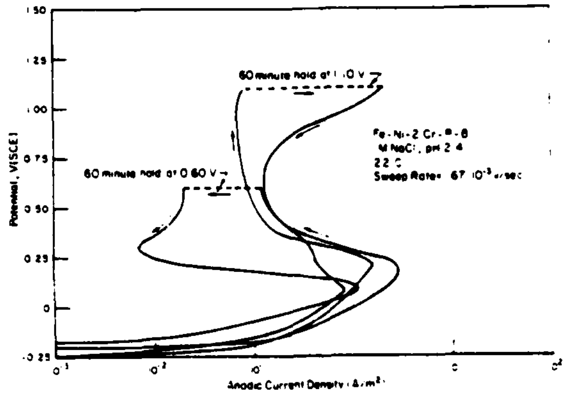

FIGURE 10 – Potentiodynamic/potentiostatic polarization curves for the 2 At.% Cr amorphous alloy.

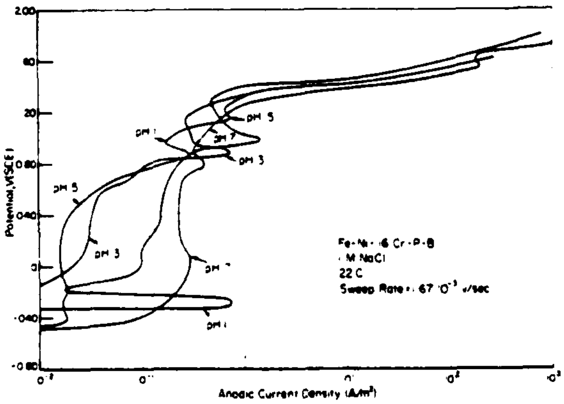

FIGURE 8 – Potentiodynamic polarization curves for the 16 At.% Cr amorphous alloy in 1M NaCl adjusted to several pH values.

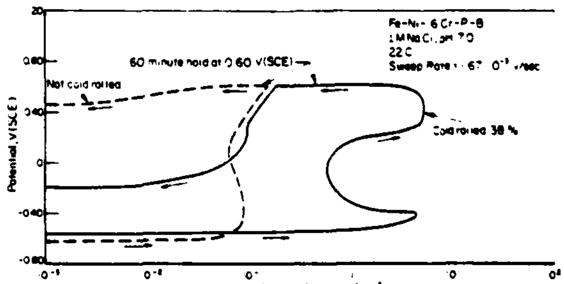

FIGURE 11 – Potentiodynamic/potentiostatic polarization curves for the 16 At.% Cr amorphous alloy in the undeformed and cold rolled conditions.

and hence the possibility of OCC. The first of these requirements, *i.e.*, existence of passive behavior, is satisfied for the amorphous alloys as shown in Figures 4 and 5. The pH dependence is discussed below.

The effect of pH on polarization behavior is documented in Figures 6 through 11. Figures 6 through 8 show potentiodynamic polarization curves for BCL alloys with Cr contents of 2, 7, and 16 At.% obtained at 22 C. The effect of decreasing the pH from 7.0 to 1 is straightforward for the 2 and 7 At.% Cr alloys (Figures 6 and 7). Specifically, as pH decreased, i_c increased uniformly, although i_p exhibited no obvious dependence. Acidification of the electrolyte, therefore, intensified active dissolution, as required for the occurrence of OCC. The dependence of i_c on pH is shown in Table 3.

TABLE 3 – Dependence of Critical Current Densities for Passivation (i_c) on pH for Amorphous Alloys Polarized in 1M NaCl

Cr Content in Alloy (At.%)	pH	i_c (A/m^2)
2	7	0.40
	5	0.73
	3	1.8
	1	9.5
7	7	0.16
	5	0.26
	3	0.42
	1	4.3
16	7	0.29
	5	0.02
	3	0.03
	1	0.73

The role of pH is less clear for the 16 At.% Cr material, as shown in Figure 8. For pH values of 7, 5, and 3, decreasing the pH appeared to facilitate passivity and suppress active dissolution. For a pH of 1, however, a prominent active peak developed. It is conceivable that some of this variation was due to natural scatter in experimental results. For example, the 16 At.% Cr alloy displayed a strong tendency to passivate, and it was, therefore, difficult to activate the alloy (by cathodic polarization) and to measure reproducible active peaks. Another possibility is that differences in corrosion behavior between the two surfaces of the filaments contributed to the scatter. Perhaps abrasion prior to polarization would be a better surface pretreatment than cathodic polarization.

A comparison of polarization behavior of amorphous alloys with that of crystalline stainless steels is made in Figure 9. Results from Incoloy 800 are particularly significant, since the Fe, Ni, and Cr contents of this alloy are somewhat similar to those of the amorphous 16 Cr alloy, but Incoloy 800 is crystalline; thus, the effects of the three metallic alloy additions can be separated according to state of crystallinity and difference in alloy homogeneity. However, a more strict comparison would necessitate comparable P and B levels in the Incoloy 800 alloy as in the amorphous alloy, but such a composition was not obtainable without copious intermetallic phases being present. In essence, both crystalline alloys suffered OCC (in this case, pitting), which initiated at about 0.15 V (SCE). The occurrence of pitting in this electrolyte was expected, and it serves to emphasize the relatively greater resistance to OCC of the amorphous alloys. It is apparent that the corrosion resistance of the amorphous alloys does not derive from the particular levels or ratios of Fe, Ni, and Cr present, as evidenced by the severe pitting of the Incoloy 800. Rather, the effect is far more subtle and presumably results from the homogeneity and possibly high P levels in the amorphous materials.[4]

To summarize the data presented thus far, it has been shown that the amorphous melt spun alloys exhibit active-passive transitions in chloride solutions, and that acidification of the solutions increases the active dissolution kinetics markedly.[(3)] These facts, and the known dependency of Cr containing alloys on dissolved oxygen for maintaining passivity, can be used to predict that some degree of susceptibility to crevice corrosion, and OCC in general, may exist for the amorphous alloys. That is, depletion of oxygen within a crevice and subsequent pH decrease due to corrosion is expected to establish an active-passive cell capable of maintaining accelerated corrosion. A comparison of corrosion kinetics with crystalline stainless steels suggests, however, that the amorphous alloys should display greater resistance to OCC than the crystalline steels.

Several experiments were performed potentiostatically at various anodic potentials to assess the importance of time on the kinetics of corrosion. That is, because crevice corrosion often takes hours (or longer) to initiate, it was considered advisable to measure dissolution kinetics in simulated crevice solutions over extended time intervals. An interval of 1 hour generally provided sufficient indication of whether the alloy was passivating or beginning to lose its passive nature.

Results of potentiostatic polarization of the 2 At.% Cr alloy in pH 2.4, 1M NaCl are shown in Figure 10. It is apparent that polarization at 0.60 V (SCE) resulted in protective film growth, as evidenced by the decrease in current with increasing polarization time. No localized corrosion occurred during the 60 minute polarization period, as verified by subsequent scanning electron microscope (SEM) analysis of the specimen. Note that the potential of 0.6 V (SCE) is well anodic to that which causes pitting of the crystalline stainless alloys represented in Figure 9, yet this low chromium alloy did not undergo pitting. The potential of 1.10 V (SCE) is at the anodic end of the passive potential region (Figure 9). The current density increased from 0.08 to 2.1 A/m^2 over the 60 minute period, suggesting that pitting may have occurred. Although some positive hysteresis occurred during the return sweep, this hysteresis disappeared at 0.3 V (SCE). Examination of the specimen surface by SEM revealed no localized attack whatsoever, even though scratches on the surface had been made with 600 grit silicon carbide paper prior to polarization to penetrate any existing oxide film, and thereby to provide sites for easy initiation of OCC.

The effect of increasing the Cr content of the alloy was to dramatically increase the tendency for passivation. The addition of 16 At.% Cr caused a steadily decreasing corrosion current during potentiostatic polarization at 1.33 V (SCE), a potential well into the oxygen evolution region of polarization behavior. This specimen was not pitted during the 60 minute polarization, either.

In general, pitting could not be induced at potentials below approximately that required for oxygen evolution for any of the amorphous alloy compositions containing 2 to 16 At.% Cr. Therefore, it was not possible to observe the conventional sudden increase in dissolution current when pitting initiated, because invariably it was masked by a large current resulting from the oxidation of water. Pits in the amorphous Battelle alloys typically were randomly distributed, rapidly penetrated the filaments, and were noncrystallographic in shape.

These potentiostatic polarization experiments reinforce results obtained potentiodynamically. That is, the alloys exhibited extreme resistance to breakdown of passivity in acidified chloride solutions, even after extended polarization at potentials anodic to those that cause film breakdown on crystalline alloys. The effect of this strong tendency for passivation on crevice corrosion will be apparent in the next section.

Crevice Corrosion Experiments

It was reasoned that the most severe crevice geometry that could be formed in these alloys would result from production of microcracks in the filament surface. Such cracks, which apparently could be produced in Metglas 2826A by a cold reduction of 32%,[6] would be extremely tight and surrounded by large areas of uncracked material to act as a cathode. To determine whether microcracks would initiate localized attack of the alloys used in this study, the 16 At.% Cr alloy was cold rolled to a 38% reduction in thickness, ultrasonically cleaned in trichloroethylene and then acetone, and potentiostatically polarized in 1M NaCl at pH 7.0. Polarization was performed at 0.60 V (SCE), a potential which was expected to be sufficiently anodic to promote crevice corrosion if it would indeed occur. Results of polarizing both the cold rolled and as-spun alloys are shown in Figure 11. Cold rolling caused a large

(3) The effect of chloride concentration has not been included in this characterization of amorphous alloys. It has been demonstrated that the effect of varying the chloride ion concentration over the range 0.02 to 2.0M exerts a relatively small effect on the polarization behavior of an amorphous Cr containing alloy, namely Metglas 2826A.[5]

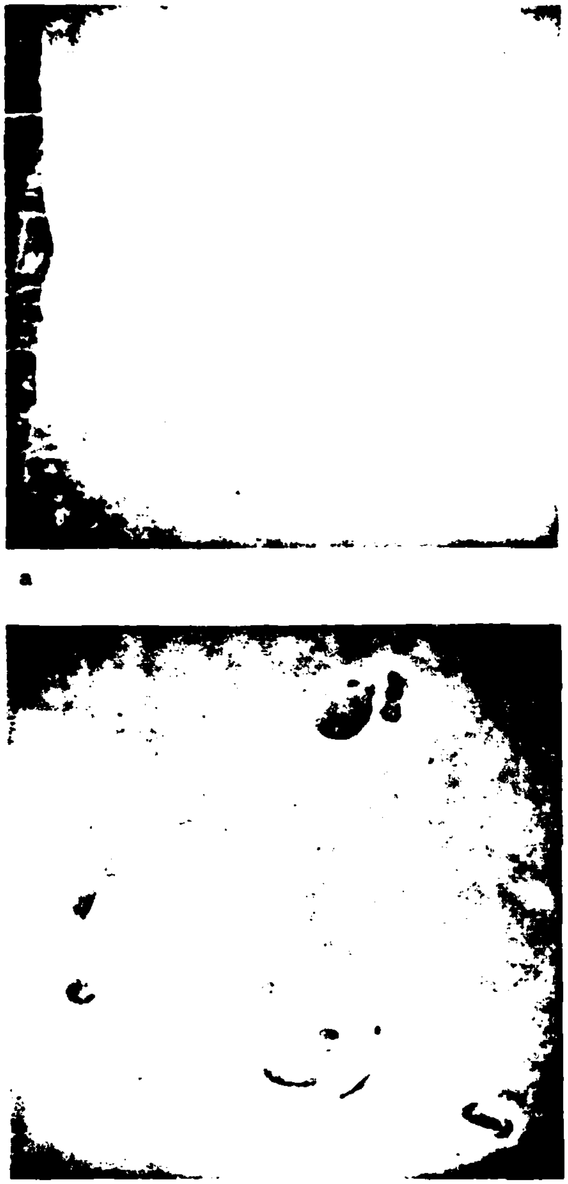

FIGURE 12 – Corrosion pits formed on the cold rolled specimen polarized as shown in Figure 11. (a) 100X, and (b) 1000X.

active dissolution peak, and it increased the passive current density significantly over that of the as-spun specimen. However, during the 60 minute hold at 0.60 V (SCE), the current density *decreased* rather than increased, the latter being expected if crevice corrosion were increasing in severity. At the end of the 60 minute period, a negative hysteresis was observed, which again was unexpected based on the assumed occurrence of crevice corrosion during the forward potential sweep.

Examination of the cold rolled specimen by SEM (Figure 12) revealed many small pits ranging up to 10 μm in diameter. The pits were never observed to penetrate the specimen. Examination of a companion specimen which was not cold rolled showed only 3 pits, and these were also less than about 10 μm in diameter. The pit density was several orders of magnitude greater on the cold rolled

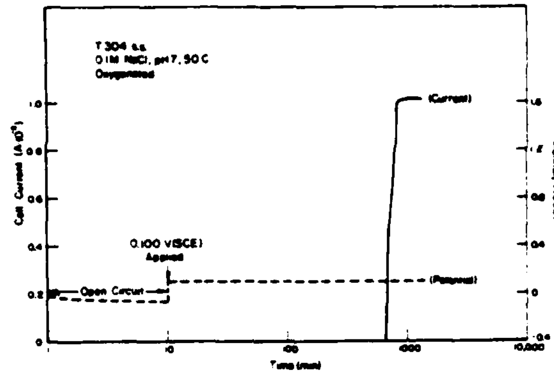

FIGURE 13 – Cell current and applied potential versus time for T304 stainless steel in the crevice test cell.

specimen.

The difference in corrosion behavior of the two materials can be rationalized as follows. Upon anodic polarization, the microcracks in the cold rolled alloy initiated crevice corrosion, and the measured anodic current density, therefore, was greater than that for the undeformed alloy. However, after the crevices had grown during the forward potential scan, during which they widened and became pit shaped, the electrolyte within each one became diluted with bulk electrolyte. By this point, about the time the 60 minute potentiostatic hold was complete, all microcracks had corroded, widened, and then passivated as bulk electrolyte mixed with that previously present in them. Previous data show that the bulk electrolyte composition of 1M NaCl at pH 7 is not sufficiently aggressive to destroy passivity at 0.60 V (SCE); hence, ingress of the electrolyte would indeed be expected to result in passivation at this potential.

The observation that crevice corrosion apparently can be forced to occur with an amorphous alloy was pursued with the crevice cell shown in Figure 2. Typical data obtained with this cell are shown in Figure 13, which depicts classical crevice corrosion of T304 stainless steel. (Total current rather than current density is plotted, because the active specimen area within the crevice was not known.) This material, known to readily undergo crevice corrosion in chloride solutions, was used initially to ensure satisfactory operation of the crevice cell. Crevice corrosion did not initiate at measurable rates under freely corroding conditions within 24 hours with this alloy, and, therefore, all experiments were performed at anodic potentials which were applied potentiostatically. (Potentials quoted are those external to the crevice.) Figure 13 indicates that about 800 minutes after a potential of 0.100 V (SCE) was applied in 0.1M NaCl at 50 C, crevice corrosion initiated. After the experiment was terminated, the crevice specimen was found to be severely corroded and the anolyte possessed a green color, presumably from Ni^{++} and Fe^{++} ions.

Figure 14 shows comparable data for the amorphous alloy containing 2 At.% Cr. Crevice corrosion occurred at an applied potential of 1.00 V (SCE), and the critical potential for crevice corrosion (E_{cc}) presumably was between 0.6 and 1.00 V (SCE). (Up to about 24 hours or 1440 minutes were allowed for initiation of crevice corrosion for these experiments. This was an arbitrary choice, made to expedite screening of alloys during these trials. Longer waiting periods might have resulted in less noble E_{cc} potentials because initiation is a time dependent process.) Note that the current attained a steady state value. The relatively short time over which the corrosion current was measured reflects the small dimensions of the filament specimen, which was rapidly dissolved *after crevice corrosion initiated.*

Figure 15 illustrates behavior for the alloy with 7 At.% Cr. It was considerably more difficult to initiate crevice corrosion with this alloy, as evident from the series of current decays following the stepwise increases in applied potential. Not until 1.50 V (SCE) was applied did a current persist for more than a few minutes. Even at

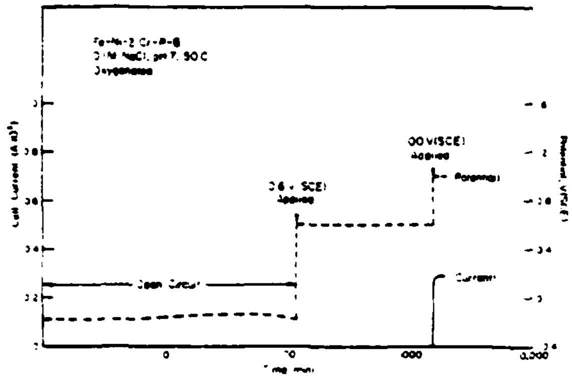

FIGURE 14 – Cell current and applied potential versus time for the 2 At.% Cr amorphous alloy in the crevice test cell.

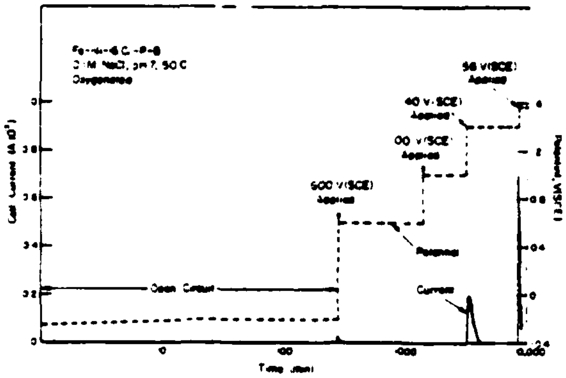

FIGURE 16 – Cell current and applied potential versus time for the 16 At.% Cr amorphous alloy in the crevice test cell.

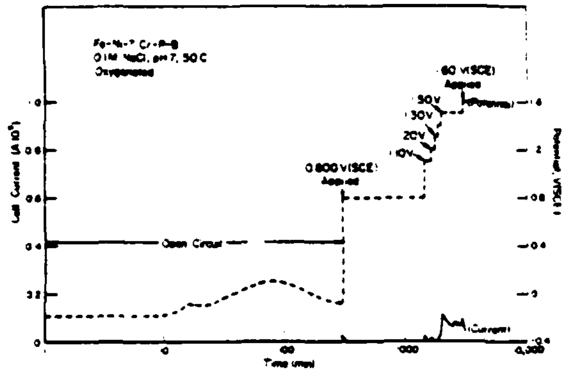

FIGURE 15 – Cell current and applied potential versus time for the 7 At.% Cr amorphous alloy in the crevice test cell.

this noble potential, the specimen exhibited a tendency to passivate, as indicated by the gradually decreasing current.

The effect of increasing the Cr level to 16 At.% is shown in Figure 16. No significant corrosion current was measured until 1.40 V (SCE) was applied. At this value, however, the alloy within the crevice passivated and the current decayed to less than 10^{-6} A. Increasing the applied potential to 1.56 V (SCE) again produced a large current transient, but the alloy was able to passivate, and the current rapidly decreased.

Additional data were generated with the crevice cell with modified specimen placement geometries. These involved placing two and three layers of amorphous alloy filament adjacent to each other within the crevice to provide a metal-to-metal interface for crevice attack to initiate. Another used a Selemion[4] anion-permeable membrane adjacent to the alloy filament to attempt to stimulate crevice attack by concentrating cations within the crevice.[11] Neither modification produced significantly different crevice corrosion behavior than the simple PTFE alloy/PTFE sandwich depicted in Figure 2. Other data were obtained with Metglas, T304 and Incoloy 800 alloys, but are not presented for brevity. Essentially, it has been shown that the amorphous alloys exhibit a markedly greater resistance to crevice corrosion than the crystalline alloys. Crevice corrosion was not observed at potentials below those required for oxygen evolution and pitting for the amorphous alloys. Their E_{cc} values are several tenths of a volt more noble than that of T304 stainless steel, a fact which is of considerable engineering significance. Essentially, the amorphous alloys exhibited the same strong tendency for passivity in the crevice cell as did freely exposed specimens in simulated crevice solutions. In this regard, the potentiostatic and potentiodynamic polarization experiments provided an accurate indication of the results of the crevice experiments: the alloys are quite passive, passivity improves with increasing Cr content, and, therefore, the alloys effectively resist localized corrosion.

However, the attack on the cold rolled alloy documented in Figures 11 and 12 is an apparent anomaly in the above reasoning. That is, it is not clear why crevice corrosion occurred in the cold rolled alloy, yet high cell currents were not measured with the crevice cell for this same alloy. One could attempt to rationalize the different results between the experiments involving cold rolled filaments and those employing the crevice cell by simply assuming that the crevice cell did not form as tight a crevice as did the microcracks. This situation could conceivably have created a more noble E_{cc} and a smaller corrosion current in the crevice cell. Nevertheless, it is still not possible to account quantitatively for the *rate* of crevice corrosion observed with the cold rolled filament. This rate can be estimated as follows. Let d equal the diameter to which a typical pit grew during the period of active growth; this period was the interval between about -0.6 V and the end of the 60 minute hold time (Figure 11), or 1.2 hours. From Figure 12, a typical pit radius (r) is seen to be about $5 \cdot 10^{-6}$ m. The corrosion current (i) required to form pits of this size over the growth period of about 1.2 hours can be approximated as[12]

$$i = \frac{r \rho F}{t E}$$

in which ρ is the alloy density (~ 8.5 g/cm^3), F is the Faraday (96,500 coulombs/equivalent), t is the growth period (1.2 hours or 4320 seconds), and E is the equivalent weight of the alloy (24.8 g/equivalent). To calculate E, the effective molecular weight of the alloy first was calculated by adding the atomic weights of the various elements present but weighted by their respective atomic fractions; this value is 49.7 g. If dissolution is presumed to occur as $M = M^{++} + 2e$, where M is predominantly Fe and Ni, then E = 24.8 g/equivalent. Use of the preceding values in the equation above results in i = 38 A/m^2. If the potential within the crevice is assumed to have been more active than that applied potentiostatically because of iR drop effects, then the maximum corrosion current that could have existed was i_c. Reference to Figures 4 and 5 shows that i_c was, respectively, $2 \cdot 10^{-1}$ A m^{-2} and 1 A m^{-2} in 1 M NaCl, pH 2.4 and in 6% $FeCl_3$, pH 1.4. These solutions should simulate reasonably well the chloride and pH conditions within crevices and pits. It is apparent that the average current density within the crevices was at least 38 times greater than the maximum observed in a simulated crevice electrolyte, namely 1 A m^{-2} in 6% $FeCl_3$.

Although the calculated average corrosion current of 38 A m^{-2} is an approximation, it is still considerably greater than the values of i_c quoted above. It thus remains to be explained quantitatively how

---

[4] Trademark, Asahi Glass Company, Ltd., Japan

more rapid corrosion rates were observed in the deformed filament than with the same alloy in the crevice cell. One conceivable explanation of this apparent discrepancy is that the intense deformation around each microcrack locally crystallized the alloy: crystallization would be expected to render the alloy more susceptible to corrosion based on previous research.[2] Or, perhaps oxygen depletion occurred to a lower level within the microcracks than was produced by nitrogen deaeration of bulk electrolytes, resulting in higher corrosion currents in the former case. A less likely possibility is that the pH and chloride levels that developed within the microcracks rendered the crevice electrolyte more corrosive than the simulated electrolytes. These various possibilities are being pursued and will be the subject of a subsequent publication.

Conclusions

Results of this research reveal several new features of OCC of amorphous alloys. Most importantly, the alloys studied were not particularly susceptible to crevice corrosion, as had originally been thought possible. Although microcracks induced by deformation were initially rapidly attacked, they widened, and then passivated. Additional experiments with an artificial crevice geometry indicated that the alloys are extremely resistant to crevice corrosion. This latter observation agrees with polarization experiments in simulated crevice electrolytes. Specifically, the alloys did not pit but exhibited passivity at potentials active to that for hexavalent dissolution of Cr in even pH 1, 1M NaCl. They are, therefore, quite stable and are expected to resist all forms of OCC at passive potentials. A significant observation is that only 2 At.% Cr are required to render an amorphous Fe-Ni-P-B alloy highly resistant to pitting and crevice corrosion, in agreement with a separate study.[1] The effect of increasing the Cr content in the alloys is to lower i_c considerably and i_p to a lesser extent, and to increase the already excellent resistance to crevice corrosion.

Acknowledgments

Thanks are due D. M. Lineman and R. E. Maringer for, respectively, skillful technical assistance and preparation of several of the melt spun alloys. The reviewers' comments were most helpful. The author is pleased to acknowledge financial support from the Office of Naval Research, Contract No. N-0014-77-C-0488.

References

1. Naka, M., Hashimoto, K., and Masumoto, T. High Corrosion Resistance of Chromium-Bearing Amorphous Iron Alloys in Neutral and Acidic Solutions Containing Chloride. Corrosion, Vol. 32, No. 4, p. 146 (1976).
2. Diegle, R., and Slater, J. Influence of Crystallinity on Corrosion Behavior of Ferrous Alloys. Corrosion, Vol. 32, No. 4, p. 155 (1976).
3. Hashimoto, K., and Masumoto, T. Extremely High Corrosion Resistance of Chromium-Containing Amorphous Iron Alloys. Rapidly Quenched Metals, Procs., Second Int. Conf. on Rapidly Quenched Metals, Edited by N. J. Grant and B. C. Giessen, p. 285 (1975).
4. Hashimoto, K., Asami, K., Masumoto, T., and Shimodaira, S. Characteristics of Passivity of Extremely Corrosion Resistant Amorphous Iron Alloys. Corrosion Sci., Vol. 16, p. 71 (1976).
5. Asami, K., Hasimoto, K., Masumoto, T., Shimodaira, S. ESCA Study of the Passive Film on an Extremely Corrosion Resistant Amorphous Iron Alloy. Corrosion Sci., Vol. 16, No. 12, p. 909 (1976).
6. Devine, T. M. Anodic Polarization and Localized Corrosion Behavior of Amorphous $Ni_{35}Fe_{30}Cr_{15}P_{14}B_6$ in Near Neutral and Acidic Chloride Solutions. J. Electrochem. Soc., Vol. 124, No. 1, p. 38 (1977).
7. Diegle, R. B. Unpublished research.
8. Yeh, H., and Maddin, R. Phase Transformations in Amorphous Fe-P-C Alloys. Rapidly Quenched Metals, Procs., Second Int. Conf. on Rapidly Quenched Metals, Edited by N. J. Grant and B. C. Giessen, p. 281 (1975).
9. Beauchamp, R. L. Polarization Characteristics of High Purity Iron-Rich Iron-Chromium-Nickel Alloys in Sulfuric Acid Solutions, PhD Dissertation, The Ohio State University, 1966.
10. Okamoto, G. Passive Film of 18-8 Stainless Steel Structure and Its Function. Corrosion Sci., Vol. 13, p. 471 (1973).
11. Suzuki, T., and Kitamura, Y. Laboratory Evaluation of Crevice Corrosion Resistance of Stainless Steels. Corrosion, Vol. 16, No. 10, p. 16 (1977).
12. Galvele, J. R., Lumsden, J. B., and Staehle, R. W. Effect of Molybdenum on the Pitting Potential of High Purity 18% Cr Ferritic Stainless Steels. J. Electrochem. Soc., Vol. 125, No. 8, p. 1204 (1978).

Printed in U. S. A

APPENDIX B

CREVICE CORROSION OF GLASSY Fe-Ni-Cr-P-B ALLOYS

Crevice Corrosion of Glassy Fe-Ni-Cr-P-B Alloys*

RONALD B. DIEGLE*

Abstract

Crevice corrosion of glassy Fe-Ni-Cr-P-B alloys in NaCl electrolyte was investigated as a means of differentiating between initiation-related and propagation-related corrosion behavior. Specimens containing deformation-induced surface microcracks experienced a transient type of crevice attack at potentials only slightly anodic to the free corrosion potential. However, the crevices widened into pit shaped voids and quickly passivated, apparently as a result of ingress of bulk electrolyte. Separate experiments with alloys cold worked in compression showed complete absence of attack at shear bands, indicating the need for microcracks for localized attack. Experiments with an electrochemical crevice cell, instrumented to record changes in anode potential and anolyte pH, required polarization above about 1 V (SCE) to cause crevice corrosion. The potentials of crevice specimens did not decrease substantially during corrosion, indicating the possible presence of a partially protective film. It was concluded that the alloys exhibit a high degree of resistance to crevice corrosion that parallels their excellent pitting resistance.

Early studies of the corrosion behavior of glassy chromium-containing alloys showed that they possess considerable resistance to pitting attack.[1-4] This resistance has been credited to their very homogeneous structure, which is free of crystalline defects such as grain boundaries, dislocations, stacking faults, and similar sites for initiation of pits. The ability of these alloys to passivate at very high rates is also thought to be important in suppressing pit initiation.[4] More recently, an investigation was performed to determine whether the localized corrosion resistance of glassy Fe-Ni-Cr-P-B alloys extends to crevice corrosion.[5] Crevice corrosion does not rely on the presence of heterogeneities in alloy structure for its initiation; therefore, an investigation was undertaken to determine whether glassy alloys would also resist crevice corrosion, or whether they would be as susceptible to this form of attack as are many conventional crystalline alloys. Results of the investigation demonstrated that the glassy alloys are very resistant to crevice attack. Anodic polarization behavior in acidified chloride solutions suggested that some degree of susceptibility to crevice corrosion can be anticipated, but that this susceptibility is usually less than that of crystalline stainless steel of comparable chromium content. Subsequent experiments with surface-precracked specimens verified that crevice corrosion does occur, but it ceases as soon as the crevices widen and passivate. Additional experiments were performed with a sandwich-type cell that created a prepared crevice on the surface of glassy filament specimens. Crevice corrosion occurred, but only at extremely oxidizing potentials exceeding about 1.4 V (SCE) for alloys containing 16 atomic percent chromium and polarized in 0.1M NaCl

This paper describes results of continued research on crevice corrosion of glassy alloys. It pursues the interesting observations that cold rolling of glassy filaments induces some degree of susceptibility, and it describes the electrochemical changes that occur within a crevice as corrosion initiates and proceeds toward steady state.

*Submitted for publication November, 1979; revised March, 1980.

*Battelle Columbus Laboratories, Columbus, Ohio.

Experimental Procedure

Materials

The alloys used in this research were the same as those described previously.[5] Their compositions were determined by wet chemical analysis and are listed in Table 1. Vanadium was present at the level of 2 atomic percent as a unintentional impurity; it is not considered to have had a significant effect on corrosion behavior at this low level. The five alloy compositions prepared at Battelle were first cast into pancake shaped ingots by conventional casting techniques involving induction melting of pure components in a controlled atmosphere. Next, 30 gram portions from each crystalline ingot were removed and melt spun into glassy filaments. The liquid impinged on a water cooled copper wheel rotating at 2550 m/minute in argon. The resulting filaments were about 800 μm wide and 30 μm thick. The filaments were evaluated by differential scanning calorimetry as a means of assessing the presence of a glassy structure. The shape, size, and number of exothermic peaks and the measured crystallization temperatures indicate that the alloys exhibited behavior typical of the transformation of glass to crystalline material.

Effects of Deformation

Localized corrosion was produced in crevices formed directly on the freely exposed surfaces of glassy filaments. These *in situ* crevices were produced by cold rolling the filaments by a reduction of up to 38%. Although the crevices could not be detected by SEM examination of surfaces of the cold rolled filaments, all experimental evidence indicates that they indeed were created during the deformation process. Corrosion also was studied on filament surfaces deformed in compression with a tool steel punch. Thinning the filaments in compression with a punch produced intense localized deformation, but without the simultaneous formation of tensile microcracks. After deformation, the filaments were ultrasonically cleaned in trichloroethylene, then acetone, and then rinsed in distilled water. They were mounted on the ends of tubular glass electrode holders and subjected to various types of anodic polarization in electrolyte containing sodium chloride.

Reprinted from CORROSION, Vol. 36, No. 7, pp. 362-368 (1980) July

TABLE 1 – *Compositions of Alloys Used in Corrosion Studies*

Preparation Technique	Source	Glassy	Fe	Ni	Cr	P	B	V(2)	Si	Mn	
			Composition, At%(1)								
Melt Spinning	Battelle	Yes	45	30	2	15	6	2			
		Yes	42	30	5	15	6	2			
		Yes	40	30	7	15	6	2			
		Yes	37	30	10	15	6	2			
		Yes	31	30	16	15	6	2			
Melt Spinning	Allied Chemical Corporation	Yes	32	36	14	12	6				
Conventional	Mill	No	69	8	20				1.2	1.7	(Type 304 stainless steel)

(1)Composition of Type 304 is nominal.
(2)*Vanadium was present as an impurity.*

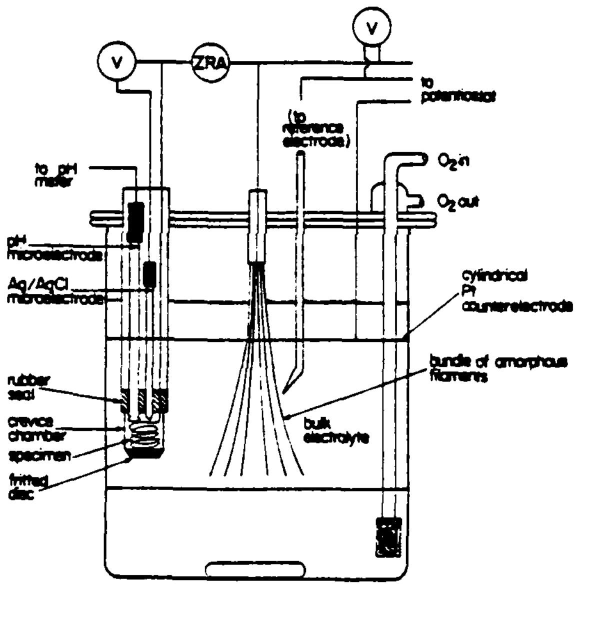

FIGURE 1 – Schematic diagram of instrumented cell used for electrochemical studies of crevice corrosion.

Electrochemical Measurements of Crevice Corrosion

A crevice cell instrumented with appropriate electrodes was used to obtain information about the electrochemical nature of crevice corrosion of glassy alloys. The cell, adapted from a similar design used by Efird and Verink,[6] is shown schematically in Figure 1. It consisted of a small crevice chamber of about one mL volume in contact with one liter of bulk electrolyte through a fine fritted disc. Inside the crevice chamber were coiled about three cm^2 of filament, which served as the anode during the crevice experiments. A silver-silver chloride ($Ag/AgCl$) micro-reference electrode and a semi micro combination pH electrode also penetrated into the crevice region, thereby enabling measurements of electrode potential and pH of crevice electrolyte to be made continuously during each experiment. An electrical lead that was soldered to the filament and masked with an acid resistant lacquer exited the crevice and was connected to a bundle of similar filaments in the bulk electrolyte through a zero resistance ammeter (ZRA). Thus, crevice corrosion current, or "cell current" flowing between the crevice specimen (anode) and external specimen (cathode), could be measured as a function of experimental parameters. The anode-to-cathode area ratio was maintained at about 1:10 throughout the experimentation.

The electrolyte used during most of the research with this cell was 1M $NaCl$. It was maintained at a pH of 7 throughout each experiment by periodic titration with appropriate amounts of dilute $NaOH$ or HCl solution. Thus, the pH of the catholyte was held constant but that of the anolyte was allowed to vary. The catholyte was also oxygenated during each experiment to insure an adequate supply of cathodic reactant. Most experiments were performed at ambient temperature, though some were performed at 85 C.

In practice, the cell was assembled and steady state conditions of electrode potential were allowed to develop. Next, the crevice and external electrodes were electrically connected through the ZRA and the resulting current flow, if any, was monitored by means of the proportional output from the ZRA. Relatively few experiments were conducted under freely corroding conditions because crevice corrosion did not occur at detectable rates in reasonable time intervals of about 24 hours. Therefore, the external electrode bundle was polarized anodically by means of an electronic potentiostat. Often, a series of potentials was applied stepwise during a single experiment, which was terminated when the crevice filaments were dissolved or corroded into several pieces.

Results and Discussion

Effects of Deformation

During the previous investigation,[5] it was reasoned that the most severe crevice geometry that could be formed in these alloys would result from production of microcracks in filament surfaces. Such cracks, which apparently had been produced in Metglas 2826A by cold rolling,[7] would be extremely tight and surrounded by large areas of uncracked material to act as a cathode. To determine whether microcracks would initiate localized attack of the alloys used in this study, a filament of glassy alloy containing 16 atomic percent Cr was cold rolled to a 38% reduction in thickness, examined by SEM, and then anodically polarized in 1M $NaCl$ at pH 7. Results of this polarization and SEM photograc of specimen surfaces are shown in Figures 2 and 3. The wavy nature of the shear bands in Figure 3 reflects the absence of crystallographic s. It was characteristic of this specimen, and all others that were cold rolled during this research program, that the surface cracks could not be

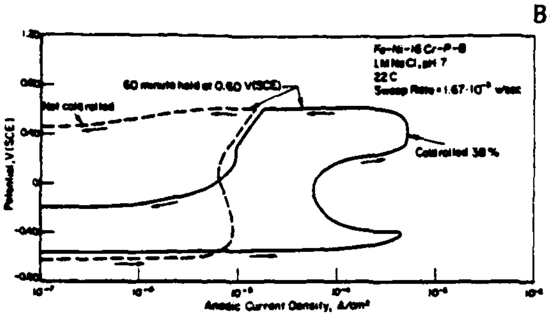

FIGURE 2 – Potentiodynamic/potentiostatic polarization curves for a 16 atomic percent Cr glassy alloy in the undeformed and cold rolled conditions (Ref. 5).

a

b

FIGURE 3 – SEM photographs of surfaces of glassy filaments containing 16 atomic percent of chromium. (a) After cold reduction by 25%, (b) after 38% cold reduction, then anodic polarization in 1M NaCl at 0.60 V (SCE) (Ref.5).

resolved microscopically. Therefore, all statements regarding their presence are made by *inference from corrosion behavior* rather than by their direct observation.

Figure 2 shows that cold rolling caused a large active dissolution peak, and it increased the passive current density significantly over that of the as-spun specimen. However, during the 60 minute hold at 0.60 V (SCE), the current density decreased rather than increased, the latter being expected if crevice corrosion were increasing in severity. At the end of the 60 minute period a negative hysteresis was observed, which was based on the assumed occurrence of crevice corrosion during the forward potential sweep.

Examination of the cold rolled specimen by SEM (Figure 3b) revealed *many small pits ranging up to 10 μm in diameter*. The pit density was several orders of magnitude greater on the cold rolled specimen.

The behavior described above was rationalized by proposing that, upon anodic polarization, the *microcracks in the cold rolled* specimen experienced transient crevice corrosion, widened, and eventually passivated. This *hypothesis was tested* in the present study in two ways. One was to polarize a cold rolled specimen in such a way as to *exhaust all sites for crevice* attack, and then determine if its *subsequent* polarization behavior returned to that of a *nondeformed specimen*. Once all microcracks had been widened by corrosion and passivated, they should not have influenced anodic polarization behavior during subsequent potential scans. To test the validity of this hypothesis, a strip of Metglas 2826A was cold rolled to about 30% reduction in thickness and polarized for one hour at 0.60 V (SCE) in 1M NaCl, pH 7. During this time, the specimen exhibited more rapid anodic dissloution relative to a nondeformed counterpart; furthermore, after polarization, the surface was heavily pitted. After examination by SEM, the same specimen was reinserted into the electrolyte and a potentiodynamic anodic polarization curve was obtained. This curve, together with one from a nondeformed filament, are displayed in Figure 4. The nearly

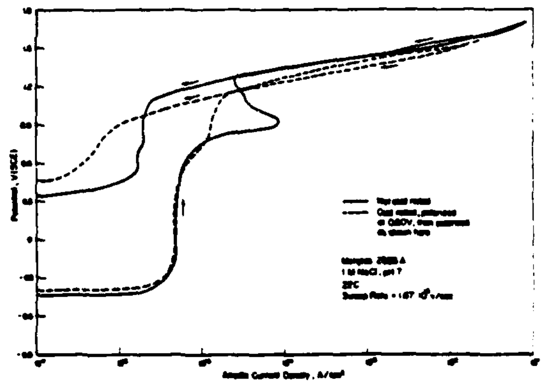

FIGURE 4 – Potentiodynamic polarization curves for Metglas 2826A in the non-cold rolled condition, and after prior potentiostatic polarization for one hour at 0.60 V (SCE) in 1M NaCl, pH 7.

coincident nature of the two curves supports the hypothesis that microcracks are the cause of the transient localized attack of cold rolled filaments. Additional evidence is presented in Figure 5, which shows the surface of cold rolled Metglas 2826A after the first (potentiostatic) polarization at 0.60 V (SCE), and another region after potentiodynamic polarization to 1.50 V (SCE) and back to the free corrosion potential. The morphology of attack, especially pit depth and number of pits per unit area, is similar for the regions shown in Figure 5(a) and 5(b), again indicating that the second polarization did not create significant new localized attack.

The foregoing represents one test of the hypothesis that surface microcracks were the cause of localized attack. However, an

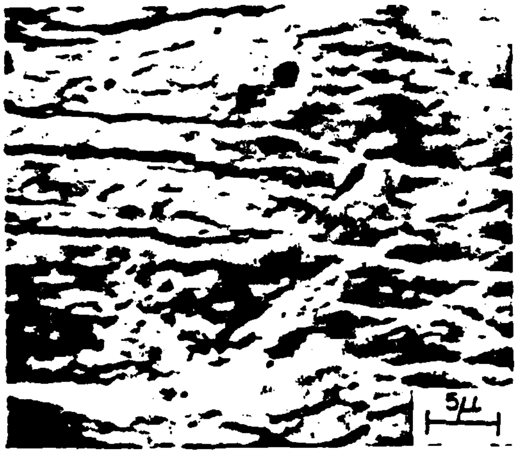

a

b

FIGURE 5 – SEM photographs of surfaces of Metglas 2826A filaments after a 25% reduction in thickness. (a) Pits formed after polarization for one hour at 0.60 V (SCE) in 1M NaCl, pH 7, (b) another region on same specimen after potentiodynamic polarization to 1.5 V (SCE) in 1M NaCl, pH 7.

a

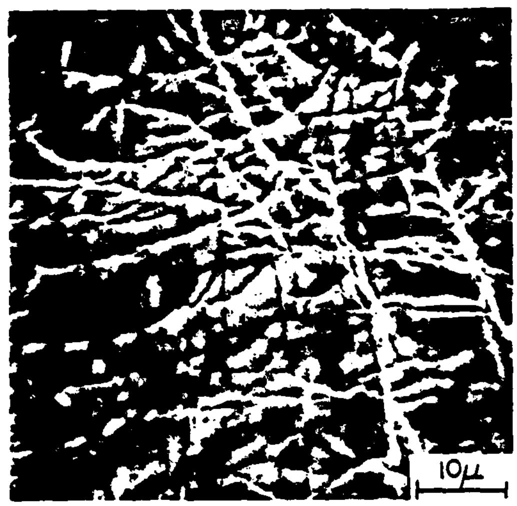

b

FIGURE 6 – SEM photographs of surfaces of Metglas 2826A that was reduced in thickness by about 10% by punching. (a) Surface after punching, (b) another region after punching, then polarizing for one hour at 0.60 V (SCE) in 1M NaCl, pH 7.

alternate explanation is that the intense cold work at certain shear bands caused localized crystallization, and that these crystalline regions experienced accelerated attack. (Metglas 2826A corrodes at very rapid rates after thermal crystallization.*) It was reasoned that intense deformation of filaments with the absence of microcrack formation should result in polarization behavior that is similar to that of nondeformed filaments if microcracks and not localized crystallization are the necessary criterion. Deformation in the absence of microcrack formation was achieved by reducing the filament thickness by compression. Specifically, filaments were cold reduced up to about 10% in thickness by impact with a tool steel punch. Punching maintained a state of local compression during deformation, unlike cold rolling, which created a state of tension on the specimen surface. Because the surface undergoing the most intense deformation was in a state of compression during punching, microcracks were not expected to develop. Results of one such experiment are presented in Figure 6, which shows deformed regions before and after polarization in 1M NaCl at pH 7. Figure 6(a) documents the fact that the punching process produced intense localized deformation, as evident by the shear bands. Figure 6(b), which is another region of the same specimen after cleaning and polarizing at 0.60 V (SCE) for one hour, shows a complete absence of pits. Thus, up to 10% plastic deformation in the absence of microcrack formation is not sufficient to produce localized attack during anodic polarization. This was verified by examining the surfaces of several specimens that had been thinned by punching and then anodically polarized; in no case was copious pitting observed such as that shown in Figure 5. (Although it was desirable to evaluate compressive strains comparable to those produced by cold rolling, attempts to produce strains greater than about 10% by punching caused the filaments to break into pieces.)

It has been shown that plastic deformation of glassy alloy filaments by rolling results in a crevice corrosion type of attack at potentials at and below 0.60 V (SCE) in neutral 1M NaCl solution. It appears that the cracks themselves, and not the deformation that accompanies crack formation, promote this attack. The crevices

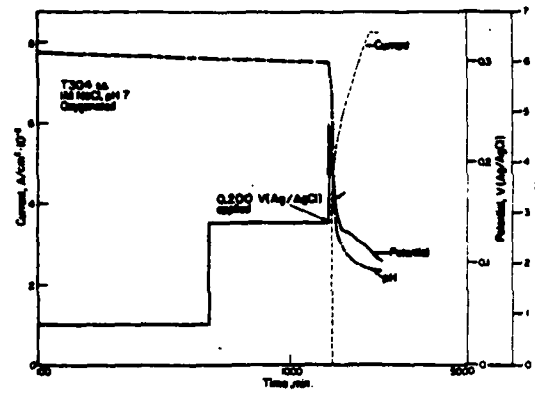

FIGURE 7 — Cell current, anode potential and anolyte pH versus time for Type 304 stainless steel evaluated in the instrumented crevice cell in 1M NaCl, pH 7, oxygenated, at 22 C.

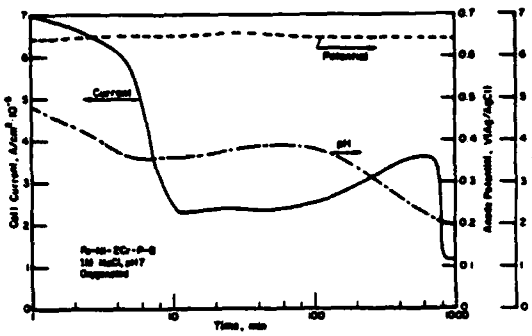

FIGURE 8 — Cell current, anode potential, and anolyte pH versus time for a 2 Cr glassy alloy evaluated in the instrumented crevice cell in 1M NaCl, pH 7, oxygenated, at 22 C.

propagated by corrosion into the alloy to depths of only a few microns, at which time they widened and passivated.

Crevice Cell Experiments

Previous research showed that the critical potential for causing crevice corrosion on cold rolled 16 Cr filaments was barely anodic to the free corrosion potential in 1M NaCl, yet it was above 1 V (SCE) in a fabricated crevice cell. Therefore, it was decided to investigate this apparent anomaly by learning more about the electrochemical conditions that develop within propagating crevices in glassy alloys.

An indication of typical data obtained from the instrumented crevice cell is shown in Figure 7 for Type 304 stainless steel. In this experiment, Type 304 stainless steel was polarized at room temperature in *1M NaCl* at a *bulk pH of 7.0* and saturated with oxygen. After polarization for 600 minutes at a potential of 0.00 V (SCE)(1) applied to the freely exposed electrode, no cell current was observed; therefore, 0.100 V (SCE) was applied and another 1000 minutes were allowed to elapse. Again, crevice corrosion was not detected as evidenced by the absence of cell current, so 0.200 V (SCE) was applied. In a matter of minutes, the cell current rose to over 8 mA/cm^2,(2) the potential of the crevice specimen decreased from 0.24 to about 0.1 V(Ag/AgCl), and the anolyte pH decreased to below 2. These changes are in agreement with electrochemical theory regarding the mechanism of crevice corrosion and occluded cell corrosion in general, and they serve to illustrate the type of information that was obtained from the instrumented cell.

Results obtained with the 2 Cr glassy alloy are typified in Figure 8. No crevice corrosion occurred at the free corrosion potential or at potentiostatically applied potentials cathodic to 0.60 V (SCE). Accordingly, that portion of the experiment occurring before the application 0.60 V (SCE) was omitted from the plot because no significant changes in current, potential, or pH occurred. Upon application of 0.60 V (SCE), the cell current density rose rapidly to over 70 μA/cm^2. However, unlike with Type 304 stainless steel, the cell current did not continue to increase. This would have indicated a loss of passivity over an ever increasing fraction of crevice area, combined with an increasing aggressiveness of the corrodent. Instead, it gradually decreased. The pH of the anolyte continued to decline, presumably the result of hydrolysis of metal cations. Interestingly, the potential of the anode did not decrease significantly below the potential of 0.60 V (SCE) that had been applied to the cathode specimen external to the crevice chamber. Anodic dissolution possibly occurred through a corrosion product film which, through its presence, was able to maintain a relatively noble potential on the anode while it was dissolving. The final sharp decrease in cell current density at about 750 minutes was caused by breakage of one of the anode filaments due to corrosion.

The influence of increasing the chromium content to 7 atomic percent is shown in Figure 9. The effects of increasing the applied

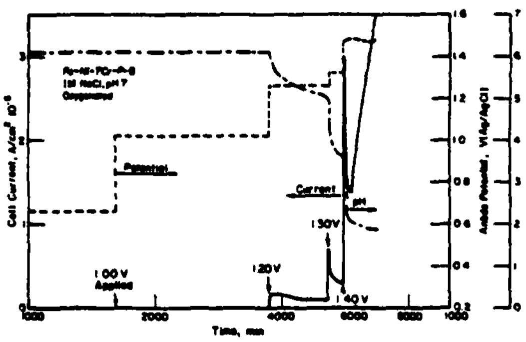

FIGURE 9 — Cell current, anode potential, and anolyte pH versus time for a 7 Cr glassy alloy evaluated in the instrumented crevice cell in 1M NaCl, pH 7, oxygenated, at 22 C.

cathode potential in a stepwise fashion are reflected in the stepwise potential increases of the anode. Measurable current did not flow until 1.20 V (SCE) was applied, after which a current transient ensued. Application of 1.30 V (SCE) produced a higher transient current, and 1.40 V (SCE) produced a still higher transient. After a few minutes had elapsed at an applied potential of 1.40 V (SCE), the cell current density suddenly increased to several hundred μA/cm^2. The solution pH at the beginning of rapid crevice corrosion was about 2. The anode potential fluctuated downward by only a few millivolts at the onset of crevice corrosion, paralleling the relatively steady potential-time behavior of the 2 Cr specimen (Figure 8). The critical crevice corrosion potential measured in this particular experiment was between 1.30 and 1.40 V (SCE).

Figure 10 shows behavior for the alloy containing 16 atomic percent chromium. Application of 1.20 V (SCE) to the cathode

(1) Potentials of the freely exposed (cathode) specimen are quoted relative to a saturated calomel electrode, SCE, whereas those of the crevice (anode) specimen are quoted relative to a silver-silver chloride electrode, Ag/AgCl. The Ag/AgCl electrode was about 40 mV more positive than the SCE, *i.e.*, 0.00 V (SCE) = 0.04 V(Ag/AgCl).

(2) All current densities are referred to the anode area, which was about 3 cm^2

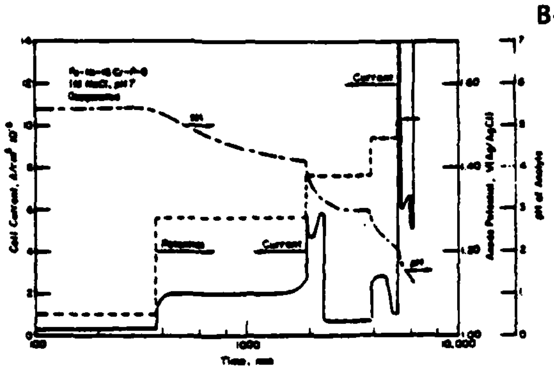

FIGURE 10 — Cell current, anode potential, and anolyte pH versus time for a 16 Cr glassy alloy evaluated in the instrumented crevice cell in 1M NaCl, pH 7, oxygenated, at 22 C.

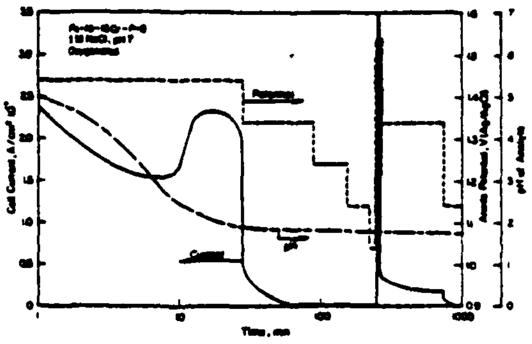

FIGURE 11 — Cell current, anode potential, and anolyte pH versus time for a 16 Cr glassy alloy evaluated in the instrumented crevice cell in 1M NaCl, pH 7, oxygenated, at 22 C.

produced cell current density of about 20 $\mu A/cm^2$, after which the the current density decreased to less than 10 ..A/cm^2. It is suspected that this very sudden decrease in current resulted from breakage of one of the several parallel strands of alloy filament in the crevice chamber. (These strands were connected in rallel and coiled inside the chamber to comprise the anode; occasionally a strand was observed to break during an experiment as a result of corrosion and the stress that accompanied coiling of the strands.) Breakage of a strand had the effect of instantaneously decreasing the total area of corroding anode, and thus of causing the cell current to fall suddenly to a lower value. In Figure 10, the fact that the cell current remained at the low value of several $\mu A/cm^2$ indicates that the was not until 1.50 V (SCE) was applied that the cell current increased, after a preliminary increase and decline, to relatively large values indicating the onset of rapid crevice corrosion. It is interesting to note that 1.40 V (SCE), even in the presence of anolyte acidified to a pH slightly less than 3, was insufficient to produce continuing crevice attack. Thus, the influence of increasing the chromium content was to confer a very arked ability of the glassy alloys to maintain a passive state, even in acidified chloride electrolytes at very oxidizing potentials.

Other experiments were performed that further emphasize the ability of glassy alloys to maintain passivity under conditions promoting crevice corrosion. One such experiment is depicted in Figure 11, which provided data on the crevice protection potential. Crevice corrosion of a 16 Cr filament was rapidly initiated in 1M NaCl by applying 1.40 V (SCE) to the cathode specimen, thus creating a cell current density exceeding 200 $\mu A/cm^2$ and a pH below 2. Next, the applied potential was decreased by 100 mV to 1.30 V (SCE), resulting in a similar shift in anode potential from 1.44 to 1.34 V (Ag/AgCl) and a decrease in cell current essentially to zero. Further decreases in potential produced no measurable effects on cell current. This cycle could be repeated, as indicated by the onset of crevice corrosion when 1.50 V (SCE) was applied to the cathode and the decrease in current when the potential was returned to less noble values. Similar trends in potential-current behavior could be produced with Metglas 2826A.

These latter experiments are significant because they demonstrate that once crevice corrosion is initiated with 14 Cr and 16 Cr glassy alloys, passivity is restored if the potential is decreased by only 100 mV below that required to initiate the attack. Thus, the difference between the crevice initiation potential and the crevice protection potential is less than about 100 mV. This is a relatively narrow span compared to those of many crystalline stainless steels, which in some cases are several hundred millivolts. The narrow range between these two potentials emphasizes the ability of glassy alloys to passivate readily once the very oxidizing potentials required to propagate crevice corrosion are removed.

Several crevice corrosion experiments were conducted at 85 C to determine whether an elevation in temperature substantially alters the behavior of these alloys. No significant differences were noted between corrosion behavior determined at 22 and 85 C. Any temperature effects were not discernable outside of the range of experimental reproducibility. The data show that even at 85 C, crevice attack occurred only at potentials above about 1 V (SCE) for the chromium-containing glassy alloys, in general agreement with experiments performed at room temperature.

Summary

The primary reason for investigating crevice corrosion of glassy alloys was to differentiate between initiation-related and propagation-related corrosion behavior. It was reasoned that crevices would provide ready made sites for initiation of localized attack, sites which do not exist on freely exposed glassy alloy surfaces because of the very homogeneous nature of the alloy structure. Measurement of susceptibility to crevice corrosion would help to determine whether the corrosion resistance exhibited by these alloys extends to propagation as well as initiation phenomena.

A study of anodic polarization showed that crevice corrosion should logically be expected to occur: the alloys exhibited enhanced corrosion at reduced electrolyte pH such as would be expected to develop during occluded cell corrosion, thus ensuring some degree of stability of active-passive cells on specimen surfaces.[5] However, the very corrosive conditions required to produce corrosion of these alloys at sensible rates indicated that the degree of susceptibility to crevice corrosion would be considerably less that that of many crystalline steels of similar chromium content, under similar exposure conditions. Subsequent experiments confirmed these predictions. Specifically, cold rolling the filaments produced a slight susceptibility to enchanced dissolution, presumably due to the formation of surface microcracks that initiated crevice corrosion. However, the depth of attack was only several μm when the crevices passivated.

Experimentation, initially with a sandwich-type crevice cell and subsequently with the instrumented cell, verified that susceptibility of the chromium-containing glassy alloys to crevice corrosion was indeed slight. Although classical crevice attack involving localized anodic dissolution and acidification of the anolyte could be made to occur, quite oxidizing (noble) potentials were required. These potentials were more than 1000 mV more noble for the 16 Cr glassy alloy than for Type 304 stainless steel. Interestingly, the potentials of glassy crevice (anode) specimens did not decrease markedly after the onset of crevice corrosion, but rather they remained within several millivolts of the potential applied to the cathode. This behavior can be interpreted as a resistance to loss of passivity, dissolution occurring instead through a film that prevailed relatively intact during crevice corrosion. This tendency to remain covered by a passive layer is in contrast to the behavior of crystalline stainless steels, which experienced a loss of passivity that increased with time

as corrosive conditions within the crevice became established. An indication of such a time-dependent activation is the large cathodic shift in electrode potential exhibited by Type 304 stainless steel in Figure 7.

This research indicates that corrosion resistance of glassy alloys extends to propagation as well as initiation of localized corrosion. The alloys exhibited an apparent strong tendency to remain covered with a passive film, which other studies have shown to be analogous in structure and composition to the hydrated chromium oxyhydroxide found on conventional chromium bearing steels.[8] It is the ability of this film to exist under extremely corrosive conditions that confers excellent corrosion resistance. This ability, in turn, presumably results from the homogeneous nature of the alloys; that is, the absence of structural defects in the alloy matrices contributes to the integrity of the film. It is probable that the chemistry of the alloys also contributes to their excellent passivity. It has been claimed that the presence of phosphorus strongly benefits this enhanced passivity, and that it confers corrosion resistance by creating rapid anodic dissolution at unfilmed sites and thereby accelerating reformation of the film; in other words, by promoting passivity.[9,10] However, results presented recently by Wang and Merz[10] have shown that extremely corrosion resistant glassy alloys can be prepared without phosphorus, thereby casting doubt on the concept that phosphorus is essential for extreme corrosion resistance. The question of the role of phosphorus and other metalloid additions on conferring passivity should be the subject of future research.

Conclusions

Glassy Fe-Ni-Cr-P-B alloys exhibited considerable resistance to crevice corrosion. This behavior parallels their demonstrated ability to resist pitting, and it reflects their extremely passive nature. Cold rolling can induce limited susceptibility to crevice attack, although the crevices propagate to depths of only several cm and then passivate. Crevice corrosion can also be produced in a prepared crevice within an electrochemical cell, although anodic polarization to oxidizing potentials exceeding about 1 V (SCE) is required to cause attack of the higher chromium alloys. During this attack, the anolyte pH decreases to below 2, but the anode potential does not activate as in the case of crystalline stainless steels. The noble nature of the anode potential during crevice corrosion is interpreted as resulting from the presence of a partially protective film that is present during dissolution. The small anodic current densities that resulted are further evidence of the presence of this film.

Acknowledgments

Thanks are due D. M. Lineman and R. E. Maringer for, respectively, skillful technical assistance and preparation of several of the melt spun alloys. The author is pleased to acknowledge financial support from the Office of Naval Research, Contract No. N-00014-77-C-0488.

References

1. Naka, M., Hashimoto, K., and Masumoto, T. High Corrosion Resistance of Chromium-Bearing Amorphous Iron Alloys in Neutral and Acidic Solutions Containing Chloride. Corrosion, Vol. 32, No. 4, p. 146 (1976).
2. Diegle, R. and Slater, J. Influence of Crystallinity on Corrosion Behavior of Ferrous Alloys. Corrosion, Vol. 32, No. 4, p. 155 (1976).
3. Hashimoto, K. and Masumoto, T. Extremely High Corrosion Resistance of Chromium-Containing Amorphous Iron Alloys. Rapidly Quenched Metals, Procs., Second Int. Conf. on Rapidly Quenched Metals, Edited by N. J. Grant and B. C. Giessen, p. 285 (1975).
4. Hashimoto, K., Asami, K., Masumoto, T., and Shimodaira, S. Characteristics of Passivity of Extremely Corrosion Resistant Amorphous Iron Alloys. Corrosion Sci., Vol. 16, No. 2, p. 71 (1976).
5. Diegle, R. B. Localized Corrosion of Amorphous Fe-Ni-Cr-P-B Alloys. Corrosion, Vol. 35, No. 6, p. 250 (1979).
6. Efird, K. D. and Verink, E. D., Jr. The Crevice Protection Potential for 90-10 Copper Nickel. Corrosion, Vol. 33, No. 9, p. 328 (1977).
7. Devine, T. M. Anodic Polarization and Localized Corrosion Behavior of Amorphous $Ni_{35}Fe_{30}Cr_{15}P_{14}B_6$ in Near Neutral and Acidic Chloride Solutions. J. Electrochem. Soc., Vol. 124, No. 1, p. 38 (1977).
8. Asami, K., Masumoto, T., and Shimodaira, S. ESCA Study of the Passive Film on an Extremely Corrosion Resistant Amorphous Iron Alloy. Corr. Sci., Vol. 16, No. 12, p. 909 (1976).
9. Naka, M., Hashimoto, K., and Masumoto, T. Sci. Rep. Res. Inst. Tohoku Univ., A286, p. 283 (1977).
10 Masumoto, T. and Hashimoto, K., Chemical Properties of Amorphous Metals. Ann. Rev. Mat. Sci., Vol. 8, pp. 215-233 (1978).
11. Wang, R. and Merz, M. D. Corrosion Resistant Amorphous Stainless Steels Containing Tungsten, presented at May meeting of The Electrochemical Society, Boston, May 6-11, 1979.

Printed in U.S.A.

APPENDIX C

CORROSION BEHAVIOR OF GLASS CHROMIUM-CONTAINING ALLOYS PREPARED BY SPUTTERING

Corrosion Behavior of Glassy Chromium-Containing Alloys Prepared by Sputtering

Ronald B. Diegle

Battelle, Columbus Laboratories, Columbus, Ohio 43201

and M. D. Merz

Battelle, Pacific Northwest Laboratories, Richland, Washington 99352

Reprinted from JOURNAL OF THE ELECTROCHEMICAL SOCIETY
Vol. 127, No. 9, September 1980
Printed in U.S.A.

C-2

Corrosion Behavior of Glassy Chromium-Containing Alloys Prepared by Sputtering

Ronald B. Diegle

Battelle, Columbus Laboratories, Columbus, Ohio 43201

and M. D. Merz

Battelle, Pacific Northwest Laboratories, Richland, Washington 99352

Glassy alloys containing Cr, P, and various other elements have been shown to possess excellent corrosion resistance by a number of workers (1-8), and were the subject of a recent review by Masumoto and Hashimoto (9). These alloys resist localized as well as general corrosion in electrolytes such as $FeCl_3$ and acidified NaCl. Furthermore, as little as 2 or 3 a/o of alloyed chromium are sufficient to confer this resistance (7). The interest in these alloys presently is of a rather fundamental nature, such as learning more about the influence of structure on corrosion and passivity. However, it is clear that glassy alloys have practical value as corrosion resistant coatings provided that a means can be developed for applying them as such.

An inherent feature of the fabrication of many corrosion resistant glassy alloys is the high quench rate, about 10^5 C/sec, necessary to attain the glassy structure upon solidification from the melt. Elaborate techniques, such as melt spinning (10) and melt extraction (11), typically are used to attain these high quench rates. A limitation of all liquid quenching techniques is that the dimension of the specimen is necessarily thin in the direction of heat extraction; typically, this dimension is about 50-75 μm, with about 125 μm a reasonable upper limit for this class of alloys. Although the filaments and narrow strips that result from liquid quenching are suitable for laboratory research studies, they cannot be utilized as coatings. Sputtering, on the other hand, is a vapor deposition technique used for coating large areas and complex geometries with thick deposits. Therefore, sputtering was investigated as a possible means for depositing extremely corrosion resistant Cr-containing alloys in the glassy state.

Experimental

The sputtering targets used during this research had the compositions $Fe_{45}Ni_{30}Cr_2V_2P_{15}B_6$ and $Fe_{31}Ni_{30}Cr_{16}V_2P_{15}B_6$. Vanadium was an impurity unintentionally added through use of a ferrophosphorus alloy. The primary variable was chromium, which was either 2 or 16 atomic percent (a/o). The alloys were prepared by melting together appropriate quantities of components in an induction furnace under an argon atmosphere, homogenizing for ½ hr, and then pouring into cyclindrical molds 13 cm in diam. Sputtering was performed at Battelle's Northwest Laboratories with triode sputtering equipment. It was performed in krypton at rates between 25 and 40 μm/hr. The substrate was copper, chilled either to −196°C or water cooled to about 15°C.[1] Three types of deposits were prepared, namely, 16 Cr sputtered onto copper at either 15° or −196°C, and 2 Cr sputtered onto copper at −196°C. The deposits were about 75 μm thick, nonporous, and extremely adherent to the substrates. For the purpose of comparison, liquid quenched specimens were prepared by melt spinning as previously described (7).

The state of crystallinity of the deposits was examined by thin foil transmission electron microscopy (TEM), selected area electron diffraction (SAD), and differential scanning calorimetry (DSC). Surface topography was characterized by scanning electron microscopy (SEM), and composition by x-ray fluorescence (EDAX). Results were compared to those obtained from glassy alloys of nearly identical composition but prepared by melt spinning. Prior to structural characterization the deposits were removed from the copper substrates by dissolving the copper in concentrated nitric acid. The deposits were not noticeably affected by this treatment.

Corrosion was measured gravimetrically with coupons exposed in 10% $FeCl_3$ solution at ambient temperature, and by potentiodynamic anodic polarization in neutral and acidified 1M NaCl solutions. Sputtered deposits were subjected to gravimetric measurements after first removing them from the copper substrates as described above. For anodic polarization the specimens were left intact on the copper, which was masked with an acid resistant stop-off lacquer.

Results and Discussion

Structure.—Examination of the three sputtered deposits by TEM indicated the absence of resolvable structure, in particular, microcrystalline regions and associated grain boundaries. SAD verified the absence of detectable crystallinity, as denoted by broad diffuse ring patterns. Thus, the structures of the deposits were completely glassy within the limits of resolution of these two techniques.

DSC results from sputtered and melt spun alloys are summarized in Table I. The crystallization temperatures, T_c, of sputtered *vs.* melt spun alloys differed by 11°C for the 2 Cr alloys and by 4°C for the 16 Cr alloys. The heats of crystallization, ΔQ_c, varied by about 15% for the 2 Cr alloys and by about 12% for the 16 Cr specimens. There were no obvious trends in T_c and ΔQ_c relative to the method of specimen preparation, i.e., sputtering or melt spinning. Furthermore, the effect of substrate temperature on these parameters for the 16 Cr material does not appear to be significant. It is apparent from Table I that the crystallization behavior of the sputtered 2 Cr and 16 Cr deposits approximated that of melt spun alloys of the same compositions.

Compositions of the sputtering targets and corresponding deposits were compared to determine whether

Table I. Temperatures and heats of crystallization of sputtered and melt spun glassy alloys

Chromium content, a/o	Preparation technique	Substrate temperature, °C	T_c, °C	ΔQ_c, cal/g-atom
2	Sputtering	−196	428	1273
2	Melt spinning	~15	439	1095, 1115
16	Sputtering	−196	460	1070, 1110
16	Sputtering	~15	464	1230
16	Melt spinning	~15	461	1095, 1115

Key words: pitting, passivity, amorphous, melt-spinning.

[1] For convenience the copper substrate temperatures are referred to either as −196° or 15°C. In actual fact the temperatures may have been somewhat higher because of the heat dissipated during the sputtering process.

enrichment or depletion of any elements had occurred during sputtering. Variations in concentration between target and deposit were generally 1 a/o or less. An exception was the chromium content of the nominal 16 Cr alloy, which was 2.3 a/o higher in the deposit. An important observation is that phosphorus was not depleted in the deposit. Since phosphorus is needed to achieve the glassy state and to enhance corrosion resistance, it is significant that it can be sputtered at a concentration that is close to that in the target. No information could be obtained about the initial and final concentrations of boron, since quantification of boron by EDAX was not possible.

Surface topography.—The surfaces of sputtered specimens contained numerous hillock-shaped mounds. Figure 1 shows SEM photographs of the as-sputtered surfaces of several deposits. Figure 1(a) shows these *hillocks*, which were present to a greater or lesser degree on all sputtered specimens. Figure 1(b) is a higher magnification view of these features. Although still present, the hillocks were smaller and fewer on the 16 Cr specimen sputtered onto a water-cooled substrate, Fig. 1(c). This behavior agrees with prior sputtering experience with other alloys, *i.e.*, that warmer substrate temperatures favor less pronounced growth features. Chromium content in the alloy did not strongly affect their formation for, as shown in Fig. 1(d), they were also present on the deposit containing 2 Cr. (Several of the larger hillocks had been broken off during handling, hence their truncated appearance.) Hillocks such as those shown in Fig. 1 were not present on melt spun filaments, although shallower, less cone-shaped mounds could be found on the shiny surfaces of the filaments.

The source of the hillocks shown in Fig. 1 is not known, although they sometimes appear on other types of sputtered alloys including crystalline alloys of considerably different compositions than those reported in the present investigation. They are thought to result from growth instabilities that occur during deposition of atoms onto a substrate. Their significance to alloy properties is not known; however, it is shown in a later section that they were not preferred sites for localized corrosion, neither did they compromise the corrosion resistance of the deposits.

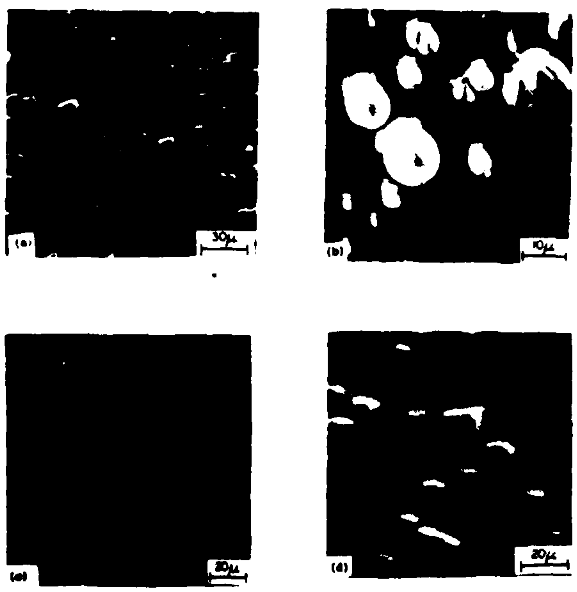

Fig. 1. SEM photographs of surfaces of sputtered deposits (a), (b) 16 Cr (LN_2 substrate); (c) 16 Cr (water-cooled substrate); (d) 2 Cr (LN_2 substrate).

Corrosion behavior.—The corrosion behavior of sputtered and melt spun specimens under freely corroding conditions was compared in 10% $FeCl_3$ solution. Data were obtained on duplicate specimens after 167 hr of exposure, and the corrosion rates were extrapolated to a μm/year basis. The corrosion rates of the 2 Cr deposits averaged 1114 μm/year, whereas those of the 2 Cr melt spun alloy averaged 427 μm/year or 38% of the former value. Analogously, the corrosion rates of the 16 Cr deposit averaged 1.8 μm/year and those of the 16 Cr melt spun alloy averaged 3.5 μm/year, or 43% of the former value. Three features are particularly noteworthy regarding these data, as follows:

(*i*) The effect of increasing the chromium concentration in the sputtered deposits was to reduce greatly the corrosion rates, in parallel with the influence of chromium in melt spun specimens.

(*ii*) Corrosion rates of the 2 Cr deposits were about two to three times greater than those of the corresponding melt spun specimens.

(*iii*) Corrosion rates of both the melt spun specimens and the sputtered deposits containing 16 Cr were relatively low, indicating that the alloys were spontaneously passive in the $FeCl_3$ solution.

Anodic polarization was used to obtain more detailed information about corrosion behavior, as shown in Fig. 2 and 3. Figure 2 shows that the 2 Cr sputtered deposit underwent an active-passive transition in 1M NaCl, pH 3, whereas the 2 Cr melt spun filament was spontaneously passive. A reaction of unknown origin gave rise to a slight active-passive transition at about −0.45 to −0.50V (SCE). The critical current density for passivation for the sputtered alloys was about 10^{-3} A/cm², and the minimum passive current density for all three specimens was about $9 \cdot 10^{-5}$ to 10^{-4} A/cm².

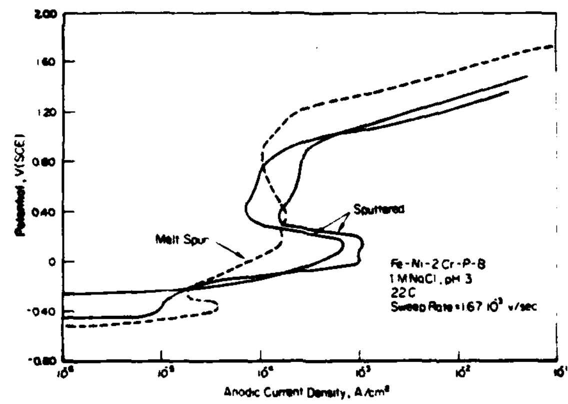

Fig. 2. Anodic potentiodynamic polarization curves of sputtered and melt spun 2 Cr alloys in 1M NaCl, pH 3, deaerated.

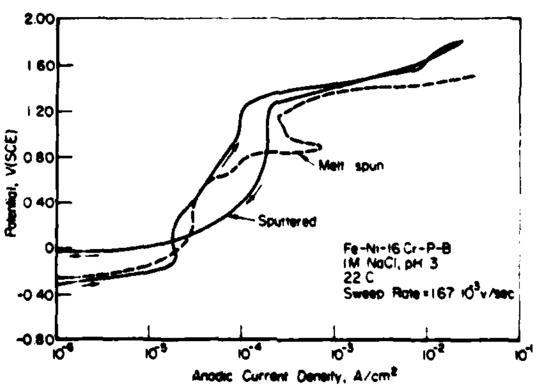

Fig. 3. Anodic potentiodynamic polarization curves of sputtered and melt spun 16 Cr alloys in 1M NaCl, pH 3, deaerated.

The steep increase in current at potentials above about 0.8V (SCE) was due to the selective oxidation of chromium as the hexavalent ion, Cr^{+6}.

As indicated in Fig. 3, the 16 Cr specimens were spontaneously passive in pH 3, 1M NaCl, with passive current densities in the approximate range of $2 \cdot 10^{-5}$ to $2 \cdot 10^{-4}$ A/cm^2. This spontaneous passivity extended even to pH 1 solutions (data not shown). The deposits exhibited passivity that was as complete, or nearly so, as that of corresponding melt spun alloys. Very significantly, the sputtered alloys resisted pitting corrosion to the same degree as those prepared by melt spinning. The positive hysteresis during the return sweep for the sputtered alloy was typical of polarization for all sputtered and melt spun specimens that were polarized to transpassive potentials. It may have been caused by temporary active dissolution in microscopic pits that formed at transpassive potentials, and then rapidly passivated at potentials in the passive region of polarization behavior.

Pitting could not be produced by polarization in the passive range of potentials, even for extended times. For example, the surface of a sputtered 2 Cr alloy that was potentiostatically polarized for 1 hr in 1M NaCl, pH 3, is shown in Fig. 4. The corrosion produced a scalloped appearance on the flat regions and no preferential attack of the hillock-shaped mounds. [The truncated tops evident in Fig. 4(b) were the result of surface damage prior to exposure to the electrolyte.] The corrosion that occurred in the passive potential range of behavior produced a sort of general attack, a surface roughening reminiscent of pits that were not able to propagate after initiating. Shallow pits were observed after potentiostatic polarization at potentials that were well into the oxygen evolution range, above about 1.3V (SCE). However, even at these very oxidizing potentials the pits that developed tended to propagate to depths of only several μm, after which they apparently passivated and new pits formed nearby. Shallow pit depths and high pit densities were a characteristic common to sputtered deposits polarized at transpassive potentials. Conversely, transpassive corrosion of melt spun filaments generally produced more through-pits and lower pit densities.

There was no substantial effect of substrate temperature on anodic polarization behavior. The polarization curves for the 16 Cr deposits sputtered at $-196°$ and 15°C were similar. Both types of deposits were spontaneously passive in 1M NaCl at pH 7 and 3, with the passive current densities of the water-cooled deposits ranging to about twice those of the liquid nitrogen-cooled specimens. However, pitting susceptibilities were unaffected, with pitting occurring only at transpassive potentials (i.e., above about 1.20V (SCE) for the 16 Cr alloys). Examination of the specimens after polarization indicated that pits were shallower on the alloy sputtered at -196°C. The effect of substrate temperature on pitting and overall corrosion behavior needs further study to better define the role of this variable on corrosion.

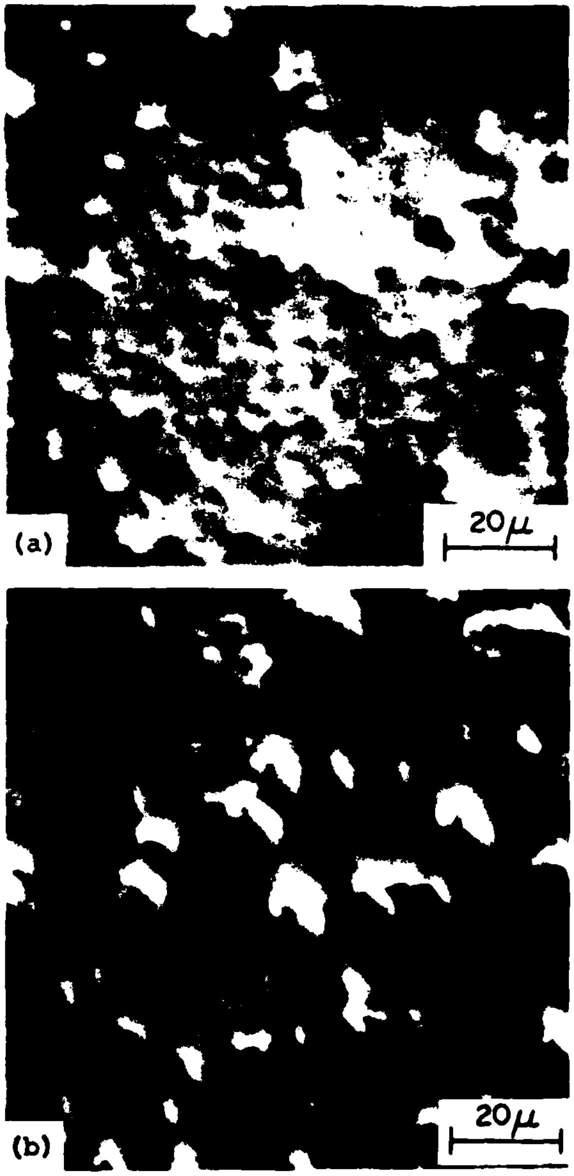

Fig. 4. SEM photographs of 2 Cr sputtered deposits polarized for 1 hr in 1M NaCl, pH 3, at the following potentials: (a) 0.60V (SCE); (b) 1.10V (SCE).

Conclusions

Sputtering can be used to prepare alloys of the Fe-Ni-Cr-P-B variety with a completely glassy structure. Thermal characteristics, such as temperatures and heats of crystallization, of sputtered alloys are similar to those of alloys of the same nominal compositions but prepared by melt spinning. Because of these similarities it is inferred that the structures of the two classes of alloys are also similar. The corrosion and electrochemical behavior of the sputtered deposits resembled, but was not identical to that of melt spun alloys of the same composition. Specifically, open-circuit corrosion rates and oxidation rates during anodic polarization of the sputtered deposits exceeded those of melt spun specimens, sometimes by about an order of magnitude. However, the sputtered deposits exhibited the same resistance to pitting corrosion as their melt spun counterparts, with pitting occurring to a large degree only at transpassive potentials in acidified chloride solutions. There is some evidence that a colder substrate temperature may favor improved corrosion resistance, but this tentative conclusion needs verification. Sputtering is a viable alternate technique for depositing extremely corrosion resistant glassy Fe-Ni-Cr-P-B alloys.

Acknowledgments

Thanks are due to D. M. Lineman and R. E. Maringer for, respectively, skillful technical assistance and preparation of the melt spun alloys. J. Brimhall of Battelle's Northwest Laboratories is credited with the TEM and selected area electron diffraction data. One of us (R.B.D.) is pleased to acknowledge financial support from the Office of Naval Research, Contract No. ONR-00014-77-C-0488.

Manuscript submitted Aug. 20, 1979; revised manuscript received March 26, 1980.

Any discussion of this paper will appear in a Discussion Section to be published in the June 1981 JOURNAL. All discussions for the June 1981 Discussion Section should be submitted by Feb. 1, 1981.

Publication costs of this article were assisted by Battelle.

REFERENCES

1. M. Naka, K. Hashimoto, and T. Masumoto, *Corrosion*, **32**, 146 (1976).
2. R. Diegle and J. Slater, *ibid.*, **32**, 155 (1976).
3. K. Hashimoto and T. Masumoto, in "Rapidly Quenched Metals," Procs., Second Int. Conf. on Rapidly Quenched Metals, N. J. Grant and B. C. Giessen, Editors, p. 285 (1975).
4. K. Hashimoto, K. Asami, T. Masumoto, and S. Shimodaira, *Corros. Sci.*, **16**, 71 (1976).
5. K. Asami, K. Hashimoto, T. Masumoto, and S. Shimodaira, *ibid.*, **16**, 909 (1976).
6. T. M. Devine, *This Journal*, **124**, 38 (1977).
7. R. B. Diegle, *Corrosion*, **35**, 250 (1979).
8. R. B. Diegle and D. M. Lineman, Technical Report No. ONR-00014-77-C-0488-2 to Office of Naval Research, May, 1979.
9. T. Masumoto and K. Hashimoto, *Ann. Rev. Mater. Sci.*, **8**, 215 (1978).
10. S. Kavesh, in "Metallic Glasses," pp. 55-70, American Society for Metals, Metals Park (1978).
11. R. E. Maringer and C. E. Mobley, in "Rapidly Quenched Metals III," pp. 49-56, The Metals Society (1978).

APPENDIX D

LISTING OF ALL TECHNICAL REPORTS, PUBLICATIONS, AND PRESENTATIONS RESULTING FROM THIS CONTRACT

APPENDIX D

Listing of All Technical Reports, Publications, and Presentations Resulting From This Contract

Technical Reports

1. Diegle, R. B., Lineman, D. M., and Boyd, W. K., "Investigating Localized Corrosion and Sputtering Feasibility of Amorphous Chromium-Containing Alloys", Interim Technical Report No. ONR-00014-77-0488 to the Office of Naval Research, April, 1978.

2. Diegle, R. B., and Lineman, D. M., "Investigating Localized Corrosion and Sputtering Feasibility of Amorphous Chromium-Containing Alloys", Interim Technical Report No. ONR-00014-77-C-0488-2 to the Office of Naval Research, May, 1979.

3. Diegle, R. B., and Lineman, D. M., "Investigating the Effects of Low Temperature Annealing Of Amorphous Corrosion Resistant Alloys", Final Report No. ONR-00014-77-C-0488-3 to the Office of Naval Research, October, 1980.

Publications

1. Diegle, R. B., "Localized Corrosion of Amorphous Fe-Ni-Cr-P-B Alloys", Corrosion, **36**(6), 250 (1979).

2. Diegle, R. B., "Crevice Corrosion of Glassy Fe-Ni-Cr-P-B Alloys", Corrosion, **36** (7), 362 (1980).

3. Diegle, R. B., Merz, M. D., "Corrosion Behavior of Glassy Fe-Ni-Cr-P-B Alloys Prepared by Sputtering", J. Electrochem. Soc., **127** (9), 2030 (1980).

4. Diegle, R. B., "Influence of Annealing on Corrosion Resistance and Ductility of Glassy Chromium-Containing Alloys", in preparation.

Presentations

1. Diegle, R. B., "Simulated Crevice Corrosion of Amorphous Fe-Ni-Cr-P-B Alloys", NACE's Corrosion/78, Houston, March (1978).

2. Diegle, R. B., "Corrosion of Metallic Glasses", TMS-AIME symposium, St. Louis, October (1978).

3. Dahlgren, S. D., presentation of selected research results at the Third International Conference on Rapidly Quenched Metals, Sussex, July (1978).

4. Diegle, R. B., and Merz, M. D., "Localized Corrosion Behavior of Amorphous Chromium-Containing Alloys", NACE's Corrosion/79, Atlanta, March (1979).

5. Diegle, R. B., and Merz, M. D., "Corrosion and Structural Characterization of Amorphous Fe-Ni-Cr-P-B Alloys", The Electrochemical Society, Boston, May (1979).

6. Diegle, R. B., "Corrosion of Amorphous Alloys", NACE (Canadian Region) Ottawa Conference, Ottawa, October (1979).

7. Diegle, R. B., "Localized Corrosion Behavior of Amorphous Chromium-Containing Alloys", The Electrochemical Society, Los Angeles, October (1979).

8. Diegle, R. B., "Localized Corrosion Research in Metallic Glasses", the Annual Meeting of the Materials Research Society, Boston, November (1979).

9. Diegle, R. B., "Influence of Structure on the Corrosion of Amorphous Alloys", American Society for Metals (Columbus Chapter), Columbus, May (1980).

10. Diegle, R. B., "Localized Corrosion of Amorphous Fe-Ni-Cr-P-B Alloys", Exxon Research Laboratory, Linden, New Jersey, July (1980).

11. Diegle, R. B., "Localized Corrosion Behavior of Amorphous Chromium-Containing Alloys", National Bureau of Standards, Gaithersburg, Maryland, August (1980).

12. Diegle, R. B., "Influence of Structure on the Corrosion of Amorphous Chromium-Containing Alloys", Naval Research Laboratory, Washington, D.C., September (1980).

13. Diegle, R. B., "Influence of Structure on the Corrosion of Amorphous Chromium-Containing Alloys", Fourth International Conference on Rapidly Quenched Metals, Sendai, Japan, August (1981) (in preparation).

14. Diegle, R. B., "Investigation of the Effects of Annealing of Amorphous Chromium-Containing Alloys", The Electrochemical Society, Denver, October (1981) (in preparation).

DA
FIL
2 -